The operation of GAPDH as a metabolic enzyme differs between the cytoplasm and nucleus

by

Helen ShiHan Tang

A thesis submitted in partial fulfillment of the requirements for the degree of

Master of Science

Department of Biochemistry
University of Alberta

Abstract

Metabolic enzymes are active in both the nucleus and cytoplasm. While metabolism in cytoplasm is widely acknowledged for energy production, nuclear-localized metabolic enzymes are thought to modulate availability of metabolites used in epigenetics. A thorough investigation of this regulatory axis requires a deeper understanding of the native environment and enzymology of these nuclear-localized proteins. *Xenopus laevis* oocytes provide several unique advantages with allowed us to develop a top-down method for biochemical analysis of near-native enzyme activity.

The cytoplasm and nucleus of *X. laevis* oocytes can be separated while maintaining compartmental integrity in mineral oil. By homogenizing the harvested nuclei and cytoplasms in a near-native buffer, we were able to compare the native enzyme kinetics between the cytoplasmic and nuclear-localized enzymes. We focused on enzymes that produce or consume NAD(P)H which can be readily detected by non-invasive spectrophotometry, and our chosen enzyme is glyceraldehyde 3-phosphate dehydrogenase (GAPDH).

GAPDH is a classic glycolytic enzyme that is highly abundant in both the cytoplasm and nucleus. Using native-western blotting, we identified that GAPDH is present in the catalytically active homotetramers in both the cytoplasm and nucleus. Robust GAPDH activity can also be detected in whole cytoplasmic and nuclear homogenates of *X. laevis* oocytes. Taking advantage of published quantitative analysis of *X. laevis oocytes,* we were able to compare the kinetic behaviour of GAPDH by analyzing the same amounts of nuclear and cytoplasmic enzyme in the near-native reaction buffer. Our results demonstrate that the operation of GAPDH as a metabolic enzyme differs between the cytoplasm and nucleus, providing the first definitive evidence of catalytic regulation of a metabolic enzyme by nuclear as compared to cytoplasmic localization.

Preface

This thesis is an original work by Helen S. Tang. The studies, of which this thesis is a part of, have received research ethics approval from the University of Alberta Animal Policy and Welfare Committee. The protocols were approved by the University of Alberta's Animal Care and Use Committee (AUP 00000942).

The preliminary high-throughput assay protocol detecting high GAPDH activity was developed by Dr. Michael Schultz and Chelsea Gates from the Schultz Lab. All other results and figures are original work obtained in my project.

This thesis is dedicated to my parents, who supported me unconditionally, and those who have guided me in this academic journey.

Acknowledgements

I would like to express my deepest gratitude to my supervisor, Dr. Michael Schultz, and my supervisory committee members, Dr. Marek Michalak and Dr. Ing Swie Goping, for their support and guidance. Their passion, enthusiasm and dedication have become and will remain my role models. The completion of my project would not be possible without their wisdom, insight, and encouragement.

Special thanks to my past lab members, Chelsea Gates, Govind Gill and Tehzeeb Sayed, for the laughter and joy during the most frustrating troubleshooting processes.

Lastly, I would like to thank the Department of Biochemistry at the University of Alberta, where the inspiring educators and supportive staff members have shaped my unique experience for my degree.

Table of Contents

List of figures

List of abbreviations

Abbreviation(s)	Definition
1,3-BPG	1,3-Biphosphoglycerate
$A_{340\ nm}$	Absorbance at 340 nm
Ab	Antibody
ATP	Adenosine Triphosphate
BSA	Bovine serum albumin
C, Cyto	Cytoplasm
DTT	Dithiothreitol
GAP	Glyceraldehyde-3-phosphate
GAPDH	Glyceraldehyde-3-phosphate dehydrogenase
hGAPDH	Recombinant human glyceraldehyde-3-phosphate dehydrogenase
K_m	Michaelis Constant of enzyme kinetics
MQ H_2O	Milli-Q Water
MW	Molecular weight
NAD^+/NADH	Nicotinamide adenine dinucleotide (+ hydrogen)
N, Nuc	Nucleus
PAGE	Polyacrylamide gel electrophoresis
PP_i	Pyrophosphate
SDS	Sodium dodecyl sulphate
TBST	Tris-buffered saline with tween solution
V_o	Initial velocity
V_{max}	Maximum enzyme velocity

Chapter 1: Introduction

1.1 General overview

In the early 1960s, multiple studies suggested enzymes form different populations between the nucleus and cytoplasm that differ in their behaviour and activity [1]. The results of these studies were challenged with possible contamination between cell fractions and alteration in nuclei permeability during the isolation procedure. Cellular fractionations identified metabolic enzymes and intermediates in the nucleus and cytoplasm [2]. Glycolytic enzymes in these fractions exhibited higher activities in the nucleus compared to the cytoplasm. Kato and Lowry obtained similar findings in freeze-section dissected nuclei and cytoplasm of dorsal root ganglions [3]. Seven of the nine metabolic enzymes assayed had higher activity in the nucleus, showing strong evidence that 1) metabolic enzymes are active in both the nucleus and cytoplasm and 2) the activities of these enzymes differ between the two compartments.

Despite the available evidence, no follow-up investigations were conducted comparing enzyme behaviour between the nucleus and cytoplasm. The interest in enzymology has gradually shifted to the moonlighting functions of metabolic enzymes before the recent resurgence in metabolic regulation. In this project, we want to continue the investigation of nucleocytosolic enzymes by comparing their behaviour under native conditions.

One of the most prominent challenges is the difficulties met during the investigation of nuclear and cytoplasmic enzyme populations is the isolation of the two compartments while maintaining native integrity. Currently, no mammalian cells would offer such samples, and the studies were often challenged by potential contamination during isolation procedures. The volume of contamination becomes significant as the volume of the nucleus is very low, and this problem is further complicated by the presence of deep nuclear invaginations in some somatic cell types [4]. The nuclear envelope creates folds that propagate into the nucleus trapping tiny pockets of cytoplasm. Oocytes from *Xenopus laevis,* the South African clawed frogs offer a means to cleanly separate the nuclear compartment from the rest of the cell while maintaining the native environment; more specifics will be discussed in section 1.4. One of the advantages of *X. laevis* oocytes is the large volume of the harvest nucleus minimizes the impact of potential cytoplasmic contamination. The isolated of nuclei from *X. laevis* oocyte dissection does not eliminate the cytoplasmic material captured by the nuclear invaginations, but the contamination resulting from nuclear invagination and adhering cytoplasm is around 4% of the nuclear volume (Figure S1). No signals were detected when assaying an equal volume of cytoplasm for activity, allowing the observation of nuclear exclusive enzyme behaviour with high confidence.

Using the *X. laevis* oocyte cell system, we propose a method for examining the native behaviour and associative structure of nuclear and cytoplasmic proteins. Non-invasive spectrometry allows for replicable high-throughput analysis of *X. laevis* whole cell, nucleus, or cytoplasm homogenates to obtain the enzymes' kinetic parameters. Through a specific examination of glyceraldehyde 3-phosphate dehydrogenase (GAPDH), we identified that the GAPDH behaviour differs between the cytoplasmic and nuclear compartments, as well as demonstrated the potential of the *X. laevis* oocyte system for investigating native-state nucleocytosolic metabolic pathways.

1.2 Importance of the subject

In 1925, Warburg et al. noted tumours' drastic increase in glucose uptake compared to surrounding tissues [5]. Aerobic glycolysis describes the process in tumour cells where glucose is fermented to lactate despite oxygen availability. Warburg's observations were confirmed along with the discovery of variable respiration magnitudes within tumours, demonstrating both mitochondrial metabolism and aerobic glycolysis are essential for tumour growth [6]. The cause and function of this phenomenon, later termed the Warburg effect, remains a topic of debate, but this uncoupling of glycolysis from aerobic metabolism highlights and importance of metabolic control dictating disease states.

Due to the highly conserved nature of essential metabolic enzymes, these enzymes and produced metabolites also participate in moonlighting functions, many of which serve as allosteric or transcription regulators in cell growth and proliferation [7]. While most current interest lies in these moonlighting functions, enzymology is still essential in understanding metabolic control in the disease cells. For example, energy stress or hypoxia stimulates cytoplasmic Acetyl-CoA (ACSS2) translocation from cytoplasm to the nucleus near gene regulatory sequences [8,9,10]. ACSS2 then recaptures acetate released from histone deacetylation and produces a local pool of acetyl-CoA. The recycled acetyl-CoA is used for histone acetylation, leading to the maintenance of cell homeostasis or tumour development in disease states.

Rather than functioning as a regulator, the catalytic activity of ACSS2 in the nucleus directly impacts cellular growth and health. Considering metabolic activity has been observed in both the nucleus and cytoplasm, this raises the question of whether compartmentalized metabolism is responsible for maintaining or disrupting cell homeostasis. The discovery of nuclear glycogen storage and glycogenolysis contributing metabolites for histone acetylation also supports this idea [11]. We propose a robust method for accurately analyzing native enzyme kinetics in the

nuclear and cytoplasmic compartments, providing a solid foundation for future investigations into compartmentalized metabolism under native conditions.

1.3 Gap in knowledge

Studies have identified the difference in activity between enzymes in the cytoplasm and nucleus [2,3]. Many procedures that extracted the nuclear metabolite and enzymes studied often disrupted the native environment in which these molecules reside. Several challenges were brought into question if the extraction procedures would alter the permeability of the nuclear membrane, resulting in contamination artifacts. Due to the small volume of samples, the enzymology experiments often required signal amplification methods and did not have replicates. To summarize, the gap in knowledge that this thesis addresses is that it remains unclear if nuclear and cytoplasmic pools of metabolic enzymes have the same kinetic properties. As discussed in section 1.4, *Xenopus laevis* oocytes address most of the abovementioned issues. Not only can the nucleus and cytoplasm be extracted with minimal contamination, but the large volume of the oocyte samples also allows for the direct observation of substrates and products in enzymology studies using non-invasive spectrometry. Utilizing these advantages, we were able to compare the native activities of nuclear and cytoplasmic enzyme populations.

1.4 Usage of *Xenopus laevis*

X. laevis oocyte is a vertebrate model cell that enables the harvesting of near-native cytoplasms, which is currently impossible to obtain with human cells. The *Xenopus* oocytes have been used to study many aspects of vertebrate biology dating back to the nineteenth century and more recent research in developmental, cellular, and molecular biology [12,13]. Two Nobel prizes have been awarded for pivotal research conducted with the *Xenopus laevis* oocyte model: nuclear transplantation and reprogramming by Sir John Gurdon in 2012 and protein molecule-controlled cell division and maturation by Dr. Tim Hunt in 2001 [13,14,15].

X. laevis oocyte oogenesis is continuous and asynchronous; oocytes at all stages of development are always present in adult female frogs [16]. Oocytes can be grouped into six stages during maturation which can be distinguished visually. At stage one, the oocytes are transparent and 50 to 300 μm in diameter [16,17]. The stage two oocytes are opaque and white, around 300 to 450 μm in diameter. Pigmentation and vitellogenesis begin at stage III. The oocytes take on a tan or brown appearance caused by melanin production, increasing to 600 μm in diameter. Stage IV range from 600 to 1000 μm in diameter, most signified by the formation of animal (darker, brown) and vegetal hemispheres (lighter, white, or pale yellow). Vitellogenesis causes the animal-to-vegetal axis to become more pronounced. At stage V, the border between the two

hemispheres is very distinct, and the diameter ranges from 1000 to 1200 μm. Stage VI marks the end of oocyte maturation and has a characteristic 200 μm- equatorial band that is unpigmented, separating the animal and vegetal hemispheres. The yolk gradient displaces the nucleus underneath the animal pole membrane for stage V and VI oocytes. The stages mainly differ in the energy resource accumulation via vitellogenesis. For ease of dissection, stage VI oocytes were prioritized in the selection, followed by stage V if most of the oocytes were not stage VI in a selected animal.

The long history of oocyte usage in laboratory research provided well-established protocols in caring for animal colonies, surgical harvesting of samples, and cell culturing with stage V and VI oocytes. The oocyte harvesting process begins with the surgical removal of ovaries from the *X. laevis* [18]. The ovary is mechanically fragmented into smaller chunks and enzymatically defolliculated by collagenase incubation [19]. The oocytes are then placed on sandpaper to remove residual cell fragments on the oocyte surface [17]. The oocytes are then allowed to rest and recover overnight at room temperature [18,19]. Stage V and stage VI cells are visually examined for condition and selected from the remaining population for dissection, homogenization, and additional analysis.

There are several advantages to using the *Xenopus* oocyte model. Despite the amphibians being more distant genetically, the *Xenopus* genome has high synteny with the human genome and contains homologs to 90% of the identified disease genes [13,20,21]. The genomic data are available on Xenbase, a central repository database of bioinformatics for the *Xenopus* model organism [13,22]. The stage V and VI oocytes are also very robust and can easily be cultured [13,20]. These oocytes are very large, varying between 1 to 1.3 mm in diameter [20,23]. The large volume provides enough samples for multiple analyses of the materials obtained from a single cell.

Most importantly, *X. laevis* oocytes provide a means to examine isolated cytoplasm and nucleus with minimal disruption. The oocytes are immersed in mineral oil for dissection, as the mineral oil prevents the diffusion of molecules between the nucleus and cytoplasm and preserves compartmental integrity [24]. The oocyte nucleus is situated directly under the center of the animal pole membrane, and its density is lower than that of the cytoplasm. The nucleus floats upward when an incision is made on the cell membrane using sharp instruments such as needles or tweezers; the incision should be small to prevent the cellular content from spilling out and triggering additional cellular pathways due to disruptions in the cell membrane. The nucleus is then harvested using a pipette, creating a clean separation between the two

compartments. Using the above characteristics, previous studies have quantified protein concentrations of the cytoplasmic and nuclear content [25]. The quantification by Kirli *et al.* and Wühr *et al.* yielded comparable results, providing a solid foundation for a closer examination of the identified proteins.

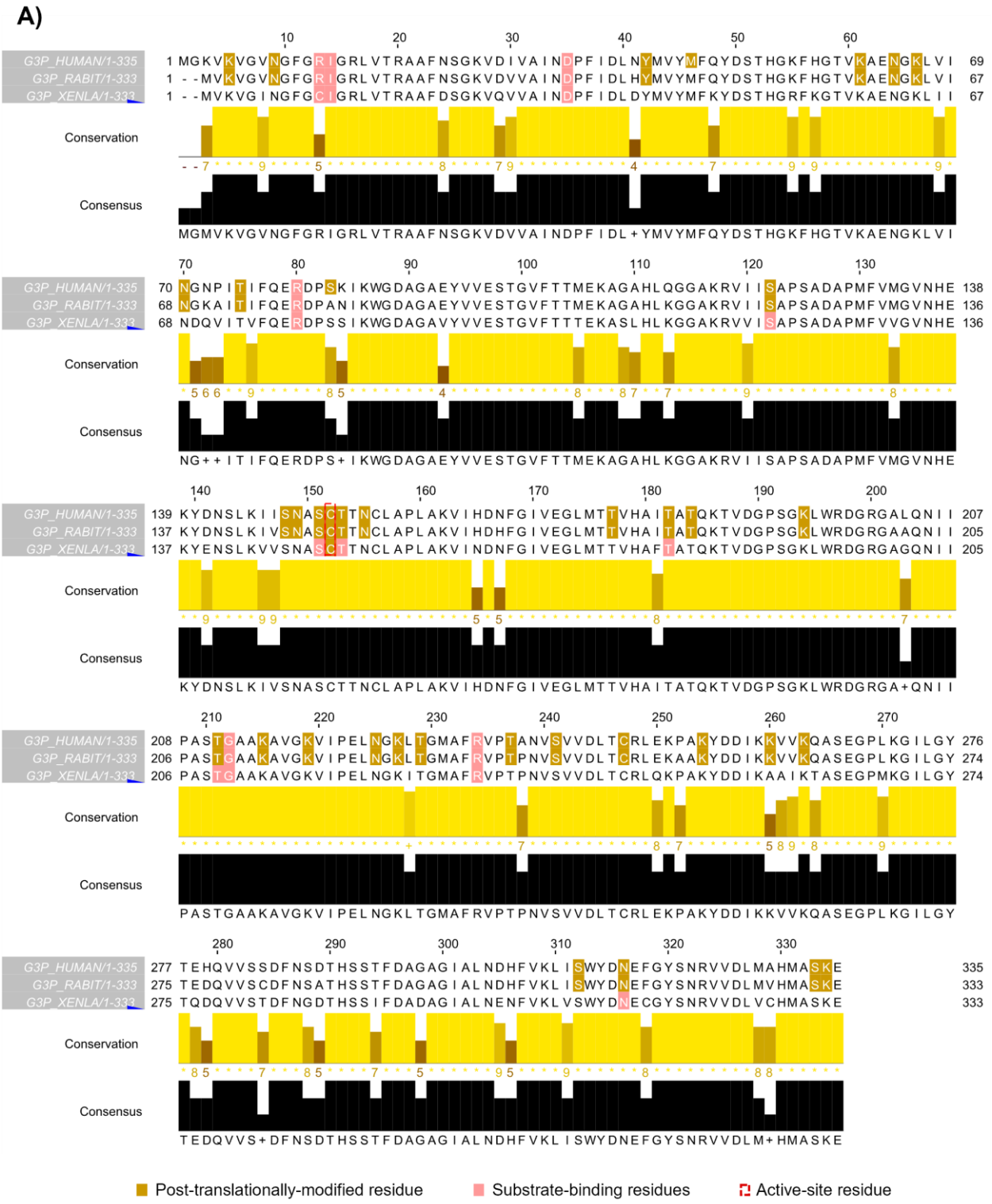

Figure 1 continued.

B)

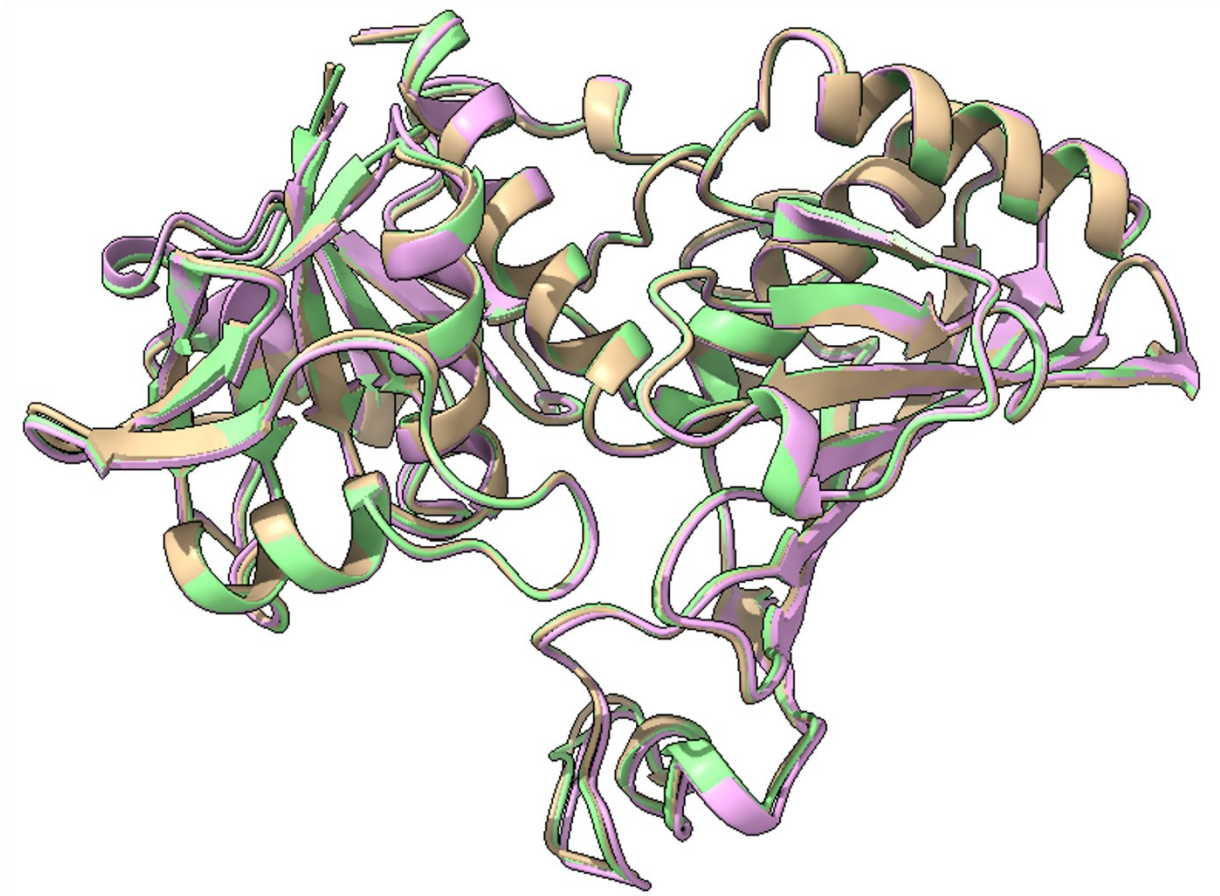

***Figure 1. GAPDH is structurally conserved through evolution*. A)** Sequence alignment of human and rabbit GAPDH to *Xenopus laevis* GAPDH. Conservation describes the similar properties of amino acids despite mutation at a certain position, and higher conservation represents higher degree of similarity; consensus describes the identity of the sequences aligned with, and higher consensus represents higher sequence identity. Sequence alignment was created using Jalview *[26]*. **B)** Structural alignment of human (yellow) and rabbit (pink) GAPDH to AlphaFold prediction of Xenopus GAPDH (green) *[27]*. Structure alignment was created using Chimera X *[28]*.

1.5 Target enzyme and hypothesis: glyceraldehyde 3-phosphate dehydrogenase (GAPDH)

Quantitative mass spectrometry data of *X. laevis* oocytes identified multiple metabolic enzymes in the nucleus and cytoplasm [18,25]. Out of all the enzymes identified, GAPDH is the most concentrated in both compartments. GAPDH is acknowledged as a housekeeping protein due to its highly conserved nature and consistent cellular expression, as shown in the sequence and

structure alignments in figure 1 [26,27,28]. This provides an opportunity for an in-depth investigation of enzyme behaviour in the nucleus [29].

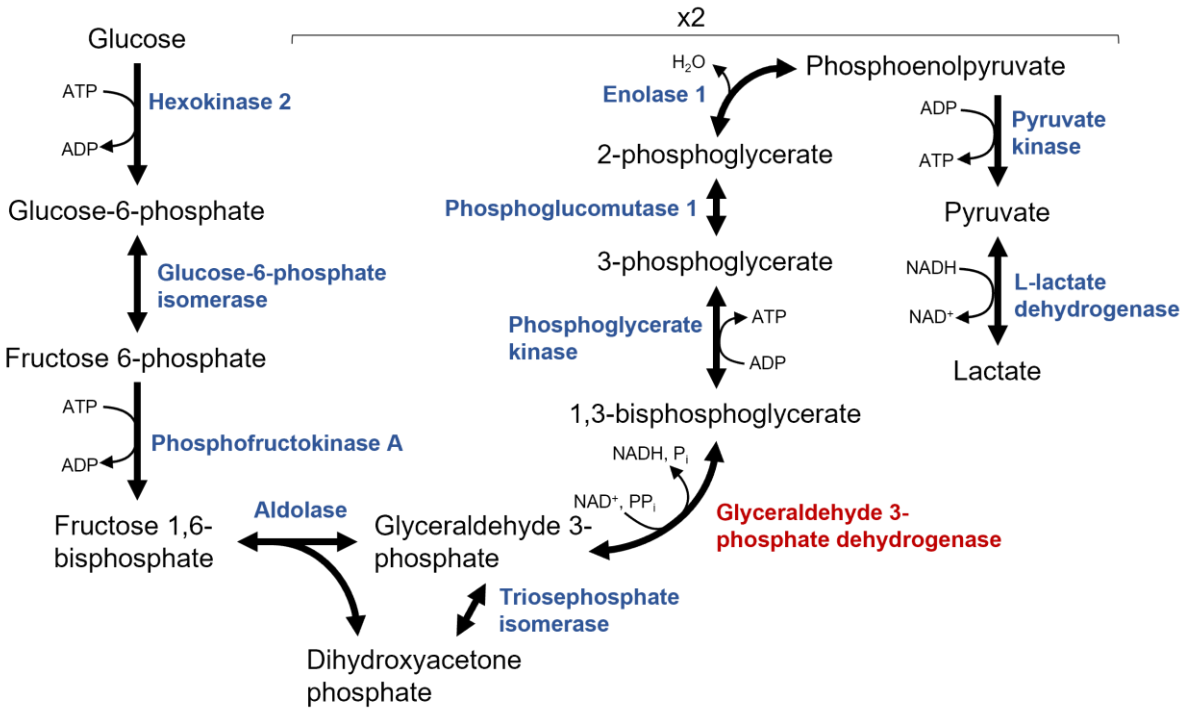

Figure 2. Schematic of enzymes and metabolites in glycolysis. All labelled enzymes were found in the quantitative protein analysis of *X. laevis* oocytes *[25]*.

GAPDH is found in multiple cellular compartments and localizations to function in various pathways. Recent reviews have summarized GAPDH moonlighting functions: Membrane-bound GAPDH participates in membrane fusion, endocytosis and iron transport; Cytoplasmic GAPDH is involved in mRNA stabilization and transport between the endoplasmic reticulum and Golgi body; Nuclear GAPDH has functions in apoptosis, transcription regulation, DNA maintenance and tRNA transport [30]. While these moonlighting functions have been of great interest, we wanted to focus specifically on GAPDH metabolic activity (Figure 2). GAPDH is post-translationally modified, some of which have been proven to impact the catalytic activity. Malonylation at K213 interferes with GAPDH mRNA binding capacity and increases the amount of free GAPDH available for metabolic catalysis [31]. GAPDH is also sensitive to the redox environment of the cell, which can dictate GAPDH reactivity [29]. Oxidation of GAPDH is often associated with loss of activity due to additional post-translational modifications [29]. For example, s-sulfuration can occur on C165 and C247, which are theorized to alter the pKa of the active site cysteine, resulting in a decrease in GAPDH activity [32]. GAPDH often accumulates in the nucleus under oxidative stress or in cancer cells [33,34]. NO-directed GAPDH S-

nitrosylation can transnitrosylate histone deacetylases (HDAC), which causes the dissociation of HDACs from chromatin resulting in enhancement of histone acetylation [35,36]. Studies also revealed that valporic acid, an HDAC inhibitor, can also inhibit GAPDH nuclear accumulation and apoptosis, hinting at GAPDH's potential role as a regulator of histone modification and chromatin organization [37].

Though GAPDH can be found in various oligomers and complexes, the enzyme itself has to be organized into homotetramers to be catalytically active [29,38]. The tetrameric formation is theorized to be promoted by NAD^+ associations or low cellular energy conditions [39]. The primary reaction catalyzed by GAPDH is well understood and described as early as 1965 [40]. GAPDH catalyzes the oxidative phosphorylation of glyceraldehyde 3-phosphate (G3P) into 1,3-bisphosphoglycerate (1,3-BPG) as part of glycolysis; the cofactor NAD^+ is reduced to NADH . G3P is the rate-determining substrate for the forward reaction *in vivo*. Arsenate functions as an acyl acceptor in place of phosphate, and it can be added to prevent the reverse reaction at equilibrium, enabling kinetic measurement of only the forward reaction. GAPDH is substrate inhibited at high concentrations of G3P and product inhibited at high concentrations of NAD^+ [40,41].

GAPDH activity is a part of aerobic glycolysis (Figure 2), and GAPDH upregulation has been observed in cancer cells [42]. Dimethyl fumarate (DMF) at high concentrations has also been identified as an inhibitor of GAPDH [43]. This inhibition of GAPDH successfully inhibited aerobic glycolysis in activated immune cells. While the GAPDH's participation in cytoplasmic metabolism is understood very well, the contrary is true for GAPDH metabolic functions in the nucleus. As mentioned in the previous sections, GAPDH and many other metabolic enzymes perform metabolite catalysis in the nucleus. But no study in the modern era has critically compared the activity of any metabolic enzyme as it occurs in the native nucleus and native cytoplasm, under near-native conditions, with knowledge of the absolute abundance of the enzyme in these compartments. We used the *X. laevis* oocyte to fill this knowledge gap through a series of experiments focused on GAPDH and hypothesize that nuclear and cytoplasmic GAPDH will exhibit different enzymatic properties in the native environment.

Chapter 2: Native-western blot identified GAPDH tetramers both in the cytoplasm and nucleus

2.1 Introduction

Sedimentary centrifugation revealed that purified GAPDH is present in dimeric, tetrameric, and octameric complexes when soluble [44,45]. Results also suggested the association and dissociation of GAPDH multimers are controlled by NAD^+ and PP_i presence. Prolonged incubation in ATP also induces dissociation of GAPDH tetramers into dimers and monomers; this dissociation is also marked by decreased GAPDH activity [39]. Activity assays conducted in conjunction with sedimentation studies indicated that the active species of GAPDH is tetrameric [44]. The tetramer formation is induced by allosteric changes upon GAPDH monomers binding to NAD^+ [29]. The presence of such tetramers suggests that GAPDH complexes are available for metabolic catalysis.

From mass spectrometry protein quantifications, GAPDH is present in the cytoplasm and nucleus at high concentrations [25]. Due to the GAPDH's potential to participate in various pathways, the oligomerization, molecule association and behaviour of GAPDH may differ between the two compartments. Higher molecular GAPDH complexes formation has been discussed in existing literature, such as the extracellular high molecular weight GAPDH found in human serum and octameric complexes addressed previously [38,39]. GAPDH can also form aggregates under oxidative stress, triggering mitochondrial dysfunction-induced cell death [46].

There is currently no insight into the native oligomerization state of GAPDH in the nucleus. We hypothesize that GAPDH will have a different tertiary structure profile between the nucleus and cytoplasm due to its participation in nuclear transport, transcription regulator and translation regulator alongside its catalytic function [29,47]. Native gel electrophoresis followed by western blotting analysis was used as an initial exploration to observe and identify any differences between the nuclear and cytoplasmic enzyme populations.

2.2 Material and Methods

Surgical extraction of the ovary, isolation of oocytes and harvesting of nucleus and cytoplasm from X. laevis. Adult female *X. laevis* (Xenopus One, MI, U.S.A) was retrieved from the animal use facility at the University of Alberta. The surgical procedures were carried out at room temperature (25℃) according to a protocol approved by the Health Sciences Animal Care and Use Committee of the University of Alberta (AUP 00000942). In preparation for ovary extraction, the animals were anesthetized using tricaine methanesulfonate, followed by

decapitation. The ovaries were then mechanically fragmented, and the oocytes were released from follicles via 2-hour collagenase incubation. The collagenase treatment had a final concentration of 3 mg/mL collagenase and 1 mg/mL bovine serum albumin (BSA) in the OR-2 medium. The OR-2 medium was taken from existing literature and contained 5 mM Hepes-NaOH pH 7.8, 82.5 mM NaCl, 2.5 mM KCl, 1 mM $MgCl_2$, 1 mM $CaCl_2$, 1 mM Na_2HPO_4 [48]. The oocytes immersed in OR-2 medium were placed on sandpaper and gently rocked to remove somatic cells still adhered to the oocyte surface [17]. The somatic cell removal was confirmed by DAPI staining (1 mg/mL) of randomly selected oocytes. The oocytes were recovered overnight and kept for up to 4 days in OR-2 buffer with penicillin and streptomycin (100 µg/mL each) as recommended in previous publications [49,50,51,52]. The healthy oocytes were selected based on established criteria: 1) evenly pigmented animal hemisphere, 2) clear border or band between animal and vegetal hemispheres, 3) no speckled or unevenly pigmented animal pole, and 4) no marks or damage [17,48,53,54].

X. laevis homogenate preparation for gel electrophoresis and western blotting analysis. Nuclei were collected in groups of 20 and homogenized in the native buffer. This buffer contains 20% glycerol and 1mM DTT in "IM with Mg^{2+}" buffer (83 mM KCl, 17 mM NaCl, 6.5 mM Na_2HPO_4, 3.5mM KH_2PO_4, 1mM $MgCl_2$) of Gall *et al.* [55]. The samples were mixed ten times using stacked pipettes in 10 µl of the native buffer. The homogenates were then brought to volume with the native buffer to a final concentration of 1 nucleus/µl, followed by a 7-second vortex to ensure thorough mixing. The cytoplasms were collected in groups of 10 and homogenized in the native buffer to a final concentration of 0.1 cytoplasm/µl. The homogenates were stored in 20 µl aliquots in -80 °C until usage.

Tris-Glycine native gel electrophoresis and western blotting of X. laevis homogenates and purified GAPDH. Bio-Rad Mini PROTEAN TGX 4-15% gels were used for native western analysis. Up to 1 nucleus and 0.1 cytoplasm and 2 µg of ProSpec human recombinant GAPDH (ENZ-350) were loaded for comparison. The gels were resolved at a constant 200V for 200 min. The gels were assembled into semi-dry transfer stacks using 1x Bio-Rad trans-blot turbo buffer with no ethanol for western blotting. The transfers were conducted using the Bio-Rad trans-blot turbo built-in high molecular weight protocol (1.3 A, 2.5 to 25 V, 10 min). Membranes were removed and blocked in 4% BSA in 1x TBST (20 mM Tris, 150 mM NaCl, 0.1% Tween 20) for one hour with gentle agitation, then washed five times in five-minute intervals with 1x TBST. The membranes were submerged in 1:5000 GAPDH monoclonal mouse antibody (D-6, sc-166545, Santa Cruz Biotechnology):4% BSA overnight for primary antibody incubation, followed by the washing procedure as described. The membranes were then

submerged for an hour at room temperature in 1:10000 goat anti-mouse IgG (H+L)-HRP conjugate (#17065516, Bio-Rad):4% BSA as the secondary incubation, followed by the washing procedure. The membrane was incubated in ECL detection reagents at a 1:1 ratio. The chemiluminescent signals were captured by exposure to film (GE Healthcare, Amersham Hyperfilm™ ELC) or by use of a Li-COR digital imager (Odyssey® XF Imaging System).

RNA digestion and agarose gel electrophoresis of X. laevis cytoplasmic homogenates. 2.5% agarose gels were made with 1x TAE buffer and Invitrogen SYBR® safe DNA gel stain. Xenopus cytoplasmic homogenates were thawed on ice, then placed on a benchtop for five minutes to equilibrate to room temperature. RNAse A (diluted with 1µg BSA/µl native buffer) was added to the homogenate and incubated for 20 minutes at room temperature for RNA digestion. A minimum of 20 µg of RNAase was required to digest the RNA in 10 µl of cytoplasmic homogenate. Digestion solutions were placed on ice until loaded on the agarose gel.

Bis-Tris native gel electrophoresis of X. laevis homogenates and purified GAPDH. Invitrogen Bis-Tris Native Gels and 1x light blue cathode buffer and 1x anode buffer (diluted from NativePAGE™ Running Buffer, BN2001 and BN2002) were used for native gel electrophoresis. Up to 0.5 nuclei, 0.05 cytoplasm, and 1 µg of ProSpec human recombinant GAPDH (ENZ-350) were loaded for comparison. PVDF membranes were presoaked in 100% ethanol (EtOH) and rinsed with MQ H_2O. The membranes were equilibrated in 1x Bio-Rad trans-blot turbo buffer with no EtOH for 15 minutes. The proteins were transferred to the PVDF membranes using Bio-Rad trans-blot turbo built-in high molecular weight protocol (1.3 A, 2.5 to 25 V, 10 min). The membranes were then fixed in 8% acetic acid. For dye removal, the membranes were air-dried and rinsed with MQ H_2O until the dye was mostly removed. Blocking, blotting and visualizing the proteins on the membrane were done as described in the Tris-Glycine native gel protocol.

Native-SDS gel electrophoresis of X. laevis homogenates and purified GAPDH. In Native-SDS gel electrophoresis, sample constituents are first separated under native conditions in the absence of SDS, and then under denaturing conditions (in the presence of SDS). 12% separating layer of the SDS gel was first poured and solidified, leaving about 5 cm to the top of the SDS gel casting apparatus. Lanes containing the sample were excised from the Tris-Glycine or Bis-Tris native gels. The excised lanes were soaked in 1x SDS loading buffer for 5 minutes before being placed horizontally at the top of the gel casting apparatus. 4% stacking layer was then poured to fill the gap between the excised native gel and the separating layer and allowed to

solidify. The SDS gel ran at a constant 150V for two hours, or 30 min, past the solvent front ran off the gel. Transferring, blocking, blotting, and visualizing the proteins on the membrane were done as described in the Tris-Glycine native gel protocol.

2.3 Results

Three approaches were used for exploring the tertiary structure of oocyte GAPDH: 1) Bio-Rad Tris-Glycine native gel system, 2) Invitrogen Bis-Tris native gel system, and 3) a 2D-system in which the lanes containing either oocyte GAPDH or purified GAPDH were excised and laid horizontally and embedded in the stacking layer of SDS-PAGE (the stacking layer did not have wells. The initial attempts at electrophoresis using the Tris-Glycine native gel system resulted in large smears when visualized via western blotting. Unsure if this resulted from GAPDH in different complexes or antibody binding to background proteins, we conducted native PAGE using the Bis-Tris gel system and 2D native-SDS electrophoresis for comparison.

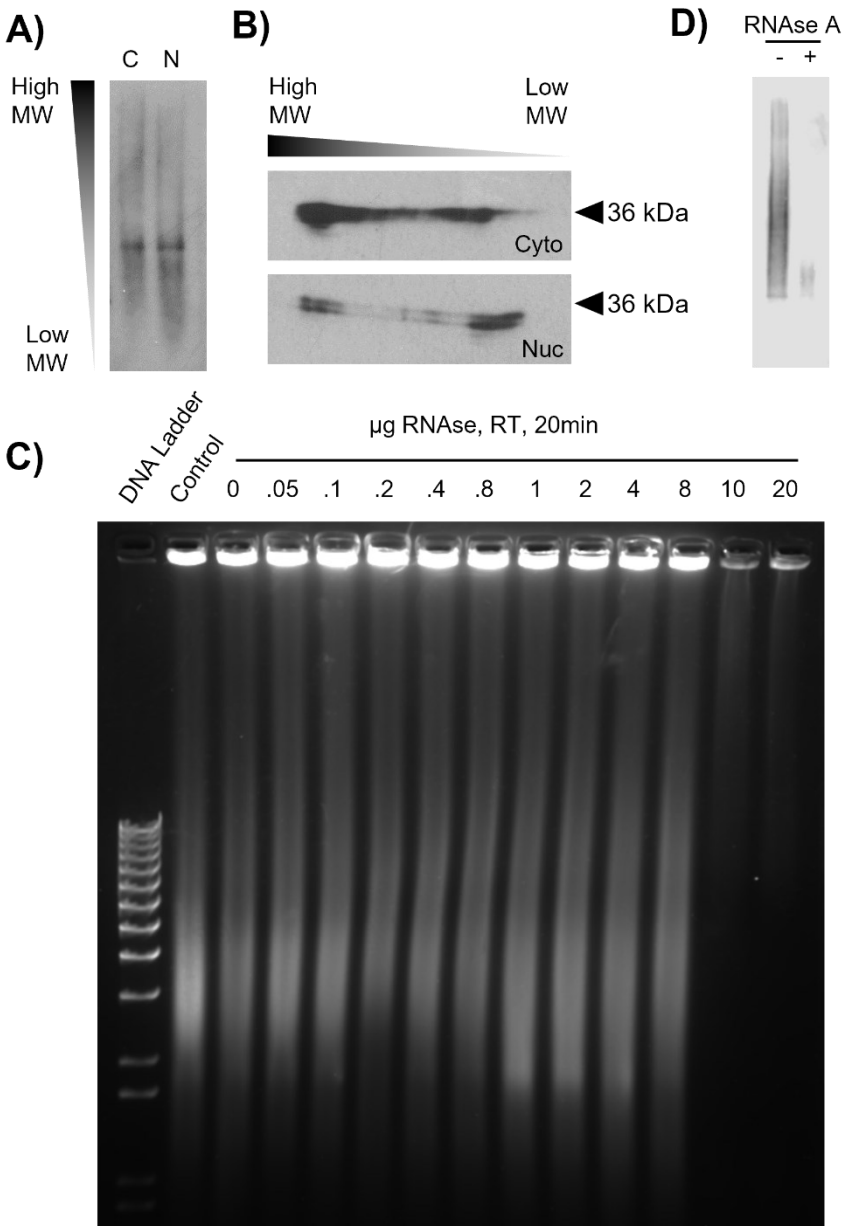

Figure 3. Xenopus cytoplasmic GAPDH is in complexes that include RNA. **A)** Tris-Glycine 4-15% native-western blotting of *Xenopus* cytoplasmic (C) and nuclear (N) homogenates. **B)** Native-SDS 2D electrophoresis of *Xenopus* cytoplasmic and nuclear homogenates. 0.1 cytoplasm and one nucleus were loaded. The western blot was visualized using Li-COR. **C)** Detection of *Xenopus* cytoplasm RNAse digestion result using 2% agarose gel. Cytoplasmic homogenates were incubated for 20 minutes at room temperature. **D)** Tris-Glycine 4-15% native-western blotting of RNAse undigested and digested *Xenopus* cytoplasmic homogenate. 0.02 cytoplasm was loaded per lane.

Native GAPDH structure in the cytoplasm and nucleus. When visualized using Bio-Rad Tris-Glycine native PAGE system, the GAPDH signal for cytoplasm was present in some discrete bands as well as a diffuse smear (Figure 3A). While the nuclear homogenate had a similar profile when analyzed with native-western, distinctive bands were seen on the native-SDS 2D electrophoresis. The native-SDS 2D electrophoresis analysis of nuclear and cytoplasmic homogenate provided two insights (Figure 3B). First, the diffuse smears in native gels are all caused by GAPDH. That is, regardless of their position in the native gel, the signal in these smears always resolved as monomeric GAPDH in the second SDS-PAGE dimension. Second, the nuclear and cytoplasmic homogenate differed in how the GAPDH signal was distributed as bands in the direction of the second dimension. Specifically, there were two distinct bands in the nuclear but not cytoplasmic homogenate. From this analysis, we concluded that the GAPDH is present in cytoplasmic complexes that were not found in the nucleus.

Influence of RNA on the migration of GAPDH in native and native-SDS 2D gels. GAPDH is known to associate with nucleic acids, including single- and double-stranded DNAs, messenger RNAs, transfer RNAs, and viral RNAs [56,57,58,59]. To assess if the GAPDH complexes in the cytoplasmic homogenates were associated with RNA molecules, we subjected the cytoplasmic homogenates to RNA digestion. The samples were loaded on 2% agarose gel and stained with Invitrogen SYBR® safe stain to visualize the nucleic acids in the homogenates. Ten microliters of cytoplasmic homogenates were incubated with various RNAse quantities at room temperature for 20 minutes for digestion and visualized in Figure 2B. The nucleic acids visualized formed long smears on the agarose gel. Compared to the freshly thawed cytoplasmic homogenate loaded in the control lane, no apparent changes were observed when compared to the homogenate that was kept at room temperature (0 μg RNA added, 20-minute incubation). This suggests that the nucleic acids in the homogenates were not degraded by molecules originally present in the cytoplasm. As more RNAse was added, a minimum of 10 μg of RNAse was required to completely remove the smear on agarose gel, suggesting the complete removal of nucleic acid molecules from cytoplasmic homogenates. We then conducted native PAGE on the non-digested and digested cytoplasmic homogenate for comparison (Figure 3C). When equal amounts of cytoplasmic homogenate were loaded, the digested homogenate contained a single diffuse band for GAPDH. From this, we concluded that the additional GAPDH complexes observed in the cytoplasmic homogenate were due to GAPDH association with RNA molecules.

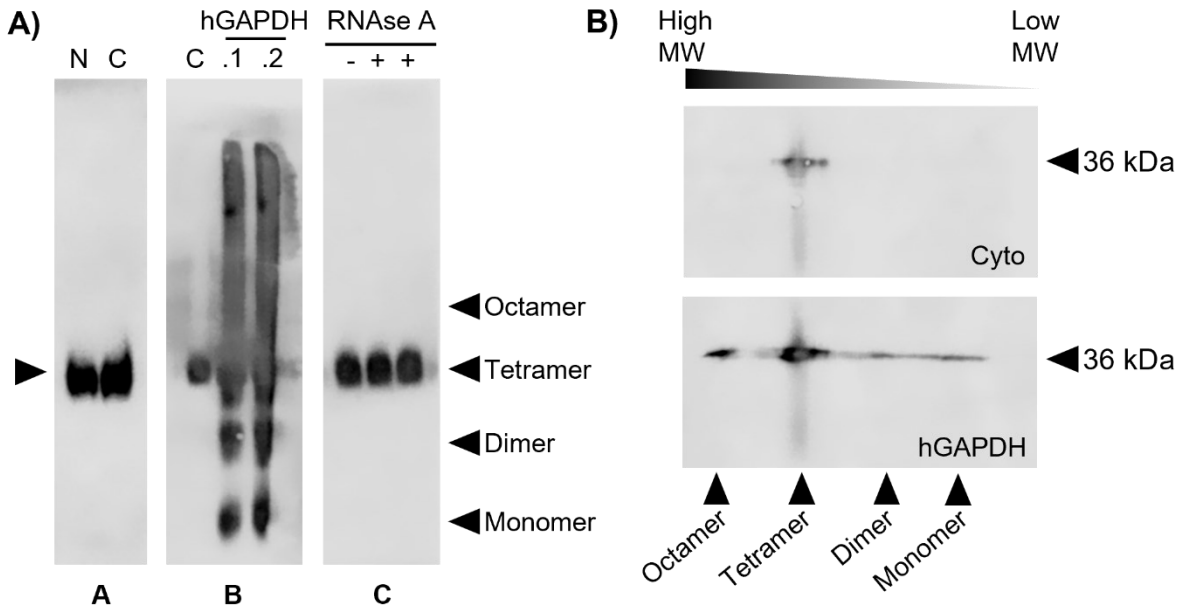

Figure 4. GAPDH forms tetramers in both the cytoplasm and nucleus. **A)** Native-western blotting of Xenopus homogenates and ProSpec purified human GAPDH. Blot A compares GAPDH bands between the nuclear (N) and cytoplasmic(C) homogenates; blot B compares cytoplasmic GAPDH and purified human GAPDH with the arrows indicating positions of GAPDH oligomers; blot C compares RNAse digested (with 10- and 20-µg RNAse, 20 min at room temperature), and non-digested cytoplasm. **B)** Native-SDS 2D electrophoresis of *Xenopus* cytoplasmic homogenate and purified human proteins. The position of each oligomer is marked by arrows.

Comparing the GAPDH in homogenate to purified GAPDH using Bis-Tris native gel system. In attempt to identify the background seen on the Tris-Glycine, we also conducted native PAGE on the *X. laevis* homogenates using the Bis-Tris gel system. Interestingly, the diffused smearing observed using the Tris-Glycine system (Figure 3A) was not observed in the nuclear or cytoplasmic homogenates (Figure 4A, blot A). GAPDH from both homogenates formed a single distinct band at the same position. Purified ProSpec human GAPDH was loaded on the Bis-Tris native gels to identify the band seen in cytoplasmic and nuclear GAPDH. The purified human GAPDH resolved into four distinct bands, corresponding to the octameric, tetrameric, dimeric, and monomeric tertiary structures from high to low molecular weight (Figure 4A, blot B). The GAPDH in cytoplasmic and nuclear homogenates resolved at the tetrameric band position when compared. Due to the high background seen at the higher molecular region of the purified human GAPDH, we again conducted native-SDS PAGE to verify the bands were caused by GAPDH (Figure 4B). Native gel bands visualized for the cytoplasmic and purified GAPDH were of proteins at the 36 kDa position when visualized with SDS PAGE, which corresponds to the molecular weight for monomeric GAPDH. No differences were

observed between RNAse digested or undigested cytoplasm. Digested and undigested cytoplasmic homogenates were loaded for comparison yielding no observable differences (Figure 4A, blot C). The Bis-Tris native gel system showed a single population of tetrameric GAPDH, which is the active tertiary structure of GAPDH, was present in the cytoplasm and nucleus.

2.4 Discussion

The Tris-Glycine native gel system identified GAPDH complexes present in the cytoplasm but not in the nucleus (Figure 3). Using RNAse digestions, we have identified the complexes formed involves RNA molecules. GAPDH does associate with nucleic acids [56,57,58,59]. It has been observed to bind to AU-rich sections and participate in the stabilization of cellular mRNAs [60]. A positive groove that spans across the NAD^+ binding pocket and dimerization interface is theorized to be the nucleic acid binding site [61,62]. NAD^+ and GAP also compete with nucleic acids in binding to GAPDH, suggesting that nucleic acid binding may compete with GAPDH available for catalytic activity. Malonylation has been identified as a post-translational modification that functions as a switch controlling GAPDH available for either mRNA binding or metabolic catalysis [31]. While RNA association could be the determining factor for alteration of GAPDH activity between the cytoplasm and nucleus, further research beyond the scope of this project is required.

We have also identified that GAPDH tetramers are both present in the cytoplasm and nucleus using the Bis-Tris native gel system (Figure 4). The reason for the different profiles detected using the Tris-Glycine and Bis-ris system is unknown, however replicates of the same analysis resulted in the same band formation. Another glycolytic enzyme that has the tetrameric active conformation and has been identified in the nucleus is pyruvate kinase. Activation of kinase receptors in cancer cells results in the phosphorylation of PKM2, causing PKM2 to dissociate into monomers from its tetrameric form [63,64]. The monomeric PKM2 is then translocated into the nucleus of cancer cells. Nuclear PKM2 has been observed to be in its dimeric form, functioning as a protein kinase as opposed to a pyruvate kinase [65]. This demonstrates how the enzymes' tertiary structure can influence their activity and function. With strong indications that GAPDH is tetrameric in the nucleus and cytoplasm, we expect to detect robust activity in both compartments (see Chapter 4).

Chapter 3: Protocol development for high throughput enzyme activity assay in the homogenates of whole cell compartments under near-native conditions

Abstract

Preliminary work in the Schultz lab revealed that high GAPDH activity could be detected in the homogenates of isolated oocyte nuclei and cytoplasms. This work was extended by refining plate assays for GAPDH so that robust estimates of K_m and V_{max} could be obtained from titrations of the substrates NAD^+ and G3P.

3.1 Introduction

GAPDH catalyzes the conversion of glyceraldehyde-3-phosphate (G3P) to 1,3-bisphosphoglycerate (1,3-BPG). The overall goal of this project was to compare the activity of the cytoplasmic and nuclear pools of GAPDH. NADH produced as a cofactor in the reaction can be measured by absorbance at 340 nm, which allows for non-invasive observation of GAPDH activity. The linear increase in A_{340} nm immediately following the addition of substrates was taken as the initial rate, and the linearity of the initial rates is highly relied upon for the accurate calculation of kinetic parameters [66]. Though whole homogenates introduce complexity, the presence of all molecular constituents of the nucleus and cytoplasm assures that the proteins will exhibit their native behaviour as closely as possible.

To examine the native behaviour of metabolic enzymes, whole Xenopus cytoplasmic and nuclear homogenates are assayed. The native buffer used for homogenization and the activity assay is based on a medium developed to study the native organization of the oocyte nucleus [55,67]. GAPDH behaved differently between pH 7.4 and pH 8.6 when examined in previous studies: K_m of NAD^+ is much higher than at pH 8.6 compared to pH 7.4, while K_m of G3P is much lower at pH 8.6 [40]. Since the native buffer we use does not match previous "standard" assay buffers, we tested if the native buffer supports the same level of activity of purified rabbit and human GAPDH as a manufacturer-recommended assay buffer. That is, we compare activity in pH 7.4 native buffer to pH 8.0 ProSpec buffer (as described in section 3.2).

We aimed to optimize the activity protocol for 96- and 384- well plates that can produce replicable linear initial rates and efficiently collect kinetic data using small volumes of samples. The large cell volume of oocytes enables the possibility of performing multiple replicate assays and different modes of analysis on the same sample, making it ideal for conducting activity assays using as few homogenate samples as possible. The challenge of creating a high-throughput activity assay with such low amounts of *X. laevis* homogenates is retaining the

linearity of initial rates. Of particular concern was the fact that whole homogenates, especially the cytoplasmic homogenate, are turbid; the turbidity could prevent the collection of reliable A_{340} measurements. Below we describe the optimization of a high-throughput measurement of GAPDH activity in nuclear and cytoplasmic homogenates under near-native conditions.

3.2 Material and methods

Preparation of stocks from purified commercial GAPDH. Recombinant human GAPDH (20 μg/μl, ProSpec, ENZ-350) was purified from *E. coli* in ProSpec buffer (20 mM Tris-Cl, 1 mM EDTA, 1 mM DTT, 20% Glycerol, pH 8.0) as noted on the company website (www.prospecbio.com/gapdh_human_active). Rabbit muscle GAPDH (lyophilized powder containing citrate buffer salts, Sigma-Aldrich G2267) was solubilized in ProSpec buffer to a final concentration of 5 units/μl. The purified enzymes are stored at -20 ℃ in small aliquots and freshly thawed for each assay.

Enzyme activity reagent stock preparation. 100 mM pyrophosphate (PP_i) and 100 mM NAD^+ were prepared by dissolving sodium pyrophosphate decahydrate (MP Biomedicals, NO. 152579) and β-nicotinamide mononucleotide (Sigma-Aldrich, N3501-25G) in the "IM with Mg2+" of Gall *et al* [55,67]. 100 mM G3P was prepared by diluting DL-Glyceraldehyde 3-phosphate solution (Sigma Aldrich, G5251-100MG) with the native buffer. The same stock solutions were also prepared in milli-Q H_2O at pH 8.0. PP_i, NAD+, and G3P were stored in -20 ℃ in small aliquots until usage. 100 mM arsenate was prepared fresh for each assay by dissolving sodium arsenate dibasic heptahydrate (Sigma-Aldrich, A6756-50G) in the native buffer.

Preparation of X. laevis cytoplasmic and nuclear homogenates. *X. laevis* oocytes were dissected under mineral oil to separate the cytoplasms and nuclei. The cytoplasms were homogenized using the native buffer (with 20% glycerol and 1 mM DTT) in groups of 40 and the nuclei in 72. The final concentration of the cytoplasmic homogenate was 1/125 cytoplasm per μl. The final concentration of the nuclear homogenates was 1/20 nucleus per μl. The homogenates were nitrogen frozen in small aliquots and stored at -80 ℃ until usage. Samples were freshly thawed for each plate assay. GAPDH concentration in these homogenates was calculated using two measurements of each cell compartment. The first was the published measurement of the absolute concentration of GAPDH the nucleus and cytoplasm of full-grown oocytes obtained by mass spectrometry [25]. The second measurement used was the volume of nucleus and cytoplasm we used to make homogenates. Photographs were taken of the nuclei and cytoplasms prior to homogenization. Since isolated nuclei and cytoplasms are spherical, the diameters of

the nuclei and cytoplasms can be measured by imaging under a light microscope with an in-field reticule. The diameters were used to calculate the volume of the nuclei and cytoplasms used for homogenization. Imaging was performed using a MZ6 dissecting microscope, IC90 E camera and Application Suite v.4.12.0 (Leica), and Chelsea Gates (Technician, Schultz lab) kindly determined the compartment volumes. The calculated concentration showed that GAPDH is four times more concentrated in our cytoplasmic homogenate than the nuclear homogenate.

High-throughput GAPDH activity assay using multi-well plates. The reaction mixture consisted of the measured GAPDH sample and 0 to 5 mM of the varying reagent for substrate titration; this makes up ¼ of the final reaction volume and contained 1 mM DTT and 20% glycerol. The reaction mix was premixed via a 7-second vortex and hand pipetted into each well in triplicates. The substrate mix contained 1 mM G3P or 3 mM NAD^+ and the constant reagents (10 mM arsenate and 5 mM pyrophosphate). 3mM NAD^+ was determined from NAD^+ titrations to provide the highest initial rate. The substrate mix was dispensed via Bio-Tek Synergy plate reader at 300 µl/s to facilitate mixing. After dispensing, the final volume of each well was 40 µl for the 384-well plate and 120 µl for the 96-well plate. The final concentration of the reaction solution in each well contained 5 mM PP_i, 10 mM arsenate, 1 mM DTT and 5% glycerol. Absorbances at 340 nm were collected in 30-second intervals using the kinetic protocol of the software that the plate reader uses (Biotek Gen 5 Microplate Reader and Imaging software). All reactions were conducted in triplicates. A340 from the initial three minutes were plotted for calculating the initial rate. Data obtained were analyzed using Microsoft Excel and GraphPad Prism.

3.3 Results

Buffer determination for high-throughput GAPDH activity assay. The manufacturer's recommended buffer for commercial enzymes is 10 mm PP_i in MQ H_2O at pH 8.0. As discussed in section 2.2, our native buffer is based on the "IM with Mg^{2+}" [55,67]. The buffer mimics the physiological nucleocytosol ion concentrations (see section 3.4 for more detail). Purified human GAPDH demonstrated higher initial rates in the pH 7.4 native buffer compared to the pH 8.0 PP_i buffer (Figure 5A), suggesting that the native buffer is a valid, if not better, buffer for assaying GAPDH activity.

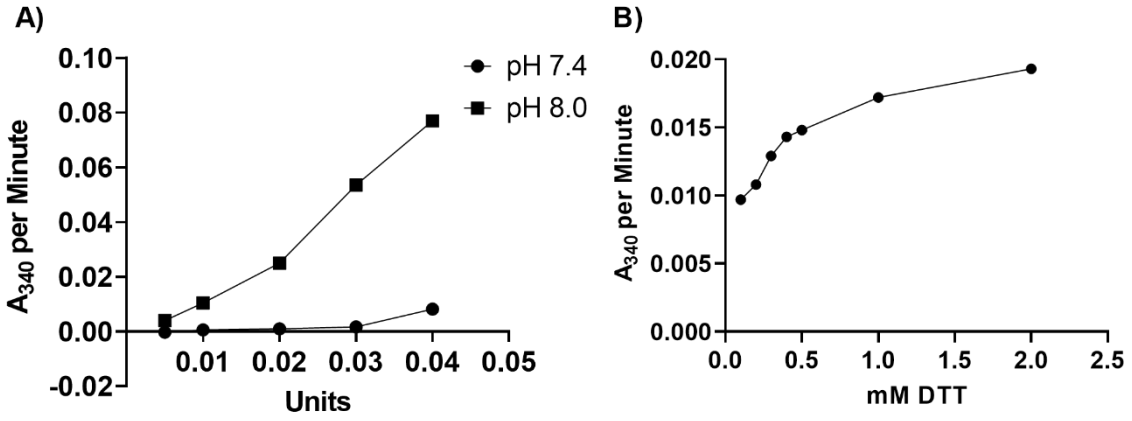

Figure 5. The activity of commercial purified GAPDH can be assayed and assessed in pH 7.4 native buffer. Control assays were performed with purified commercial enzymes and Xenopus homogenates using the 384-well plate activity assay protocol. A) Initial rates of purified human recombinant GAPDH when assayed in pH 7.4 native buffer and pH 8.0 manufacturer-recommended buffer. B) Effects of varying DTT concentration on GAPDH activity in *X. laevis* cytoplasm.

Because the cell's redox state influences GAPDH structure and activity, DTT was added to the native buffer to prevent oxidation of GAPDH [29]. While GAPDH purified from Hela cells exhibited the highest activity at 1 mM DTT [68], GAPDH in *X. laevis* homogenates exhibited higher activity with increased DTT concentrations (Figure 5B) . At higher DTT concentrations can reduce oxidated GAPDH and recover GAPDH activity [46]. In this project, the redox state of the oocytes was not measured. DTT was added with the intend to prevent further oxidation in the homogenates rather than maximize GAPDH activity. Referring to previous literature, our high-throughput plate assays contained 1 mM DTT in the final concentration [69].

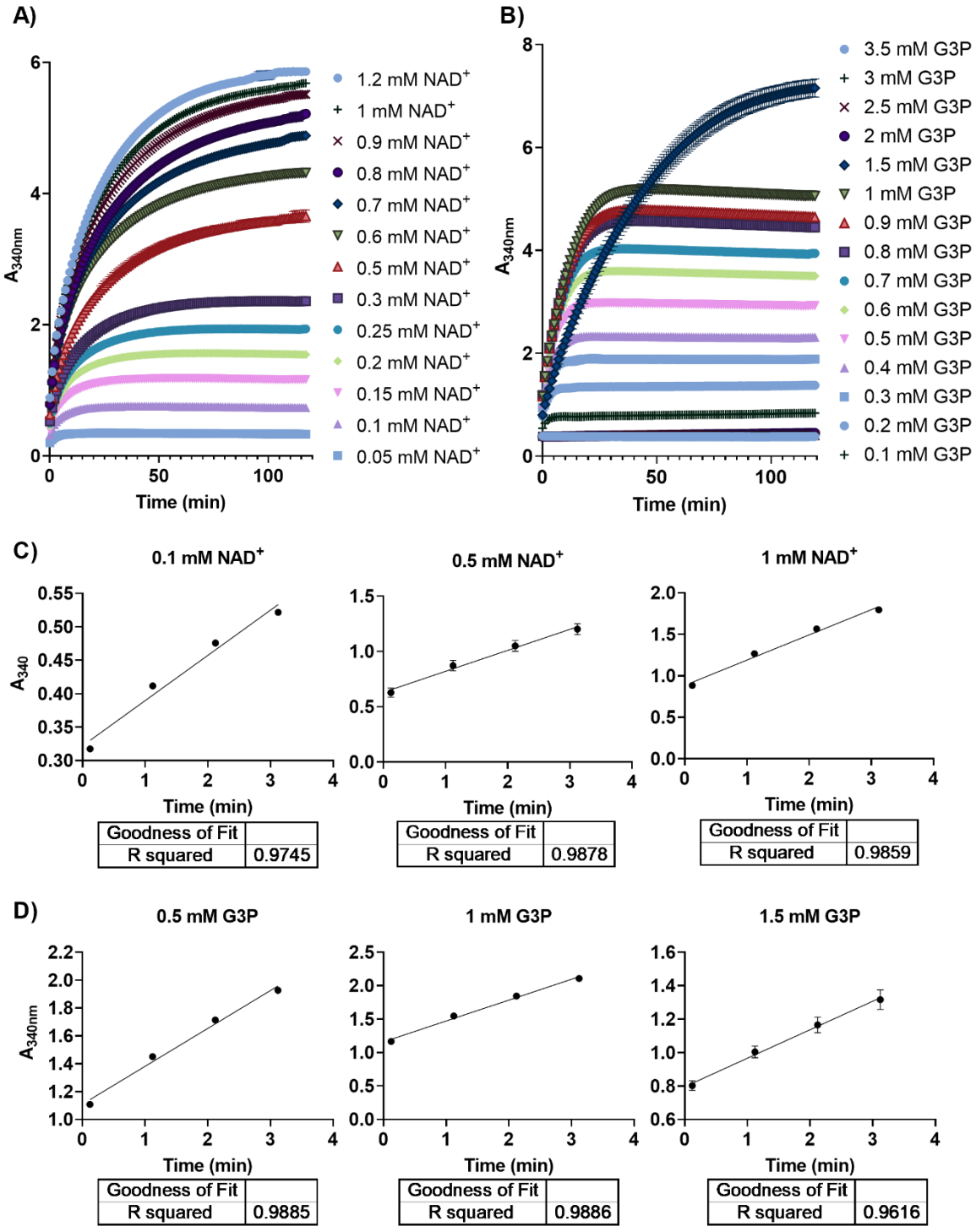

Figure 6. High-throughput activity assay was able to capture kinetic curves and initial rates for substrate titrations of purified GAPDH. **A)** Kinetic curves of NAD⁺ titration conducted on purified rabbit muscle GAPDH in pH 7.4 native buffer. **B)** Kinetic curves of G3P titration conducted on purified rabbit muscle GAPDH in pH 7.4 native buffer. **C)** Initial rates were taken from the kinetic curve for NAD⁺ titration performed on purified GAPDH shown in A). **D)** Initial rates were taken from the kinetic curve for G3P performed on purified GAPDH shown in B). The kinetic assays were conducted in triplicates, and the error bars on graphs represent the standard errors between replicates.

Analysis of GAPDH initial rate and Calculation of the Kinetic Parameters.

In this series of experiments, GAPDH initial rate was calculated under conditions of varying NAD^+ and varying G3P concentration. The high-throughput assay protocol was highly sensitive as it could detect differences in product accumulation caused by micromolar variations in substrate concentration (Figures 6A and 6B). The product accumulation during the first three minutes was taken as the initial rate. Linear fitting was performed on the A_{340} for obtaining the initial rates, and R^2 values were calculated by the Prism program to describe how well the regression line represents the data. As shown in Figures 6C and 6D, robust linearity was demonstrated in the initial rates as the R^2 value approaches 1.

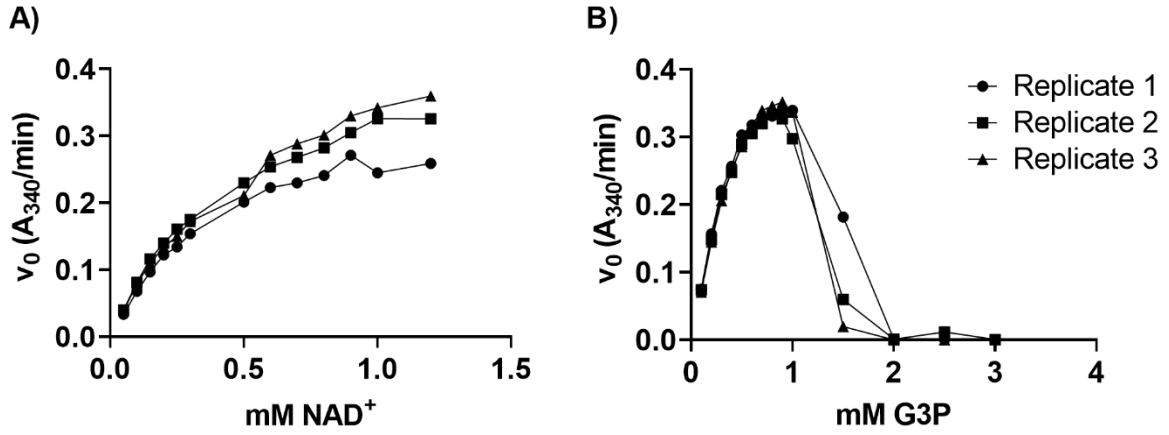

Figure 7. Michaelis-Menten Rate Curves of substrate titration performed with purified rabbit muscle GAPDH demonstrate the ideal hyperbolic shape. **A)** Rate curve for NAD^+ titration in pH 7.4 native buffer. **B)** Rate curve for G3P titration in pH 7.4 native buffer. Three replicates were carried out for each substrate titration. The average of triplicates is plotted for each replicate.

The initial rates were then plotted into Michaelis-Menten rate curves. NAD^+ and G3P titrations adhered to the ideal hyperbolic shape at lower substrate concentrations (Figure 7). The drop, or crash, in the activity of GAPDH during G3P titration is due to substrate inhibition [29]. To compare GAPDH activity, Figure 8 shows K_m and V_{max} calculation using values prior to inhibition following the analysis methods described in the review by Tummler *et al.* [70]. Estimates for the values of K_m and V_{max} were obtained by linearization of the initial rate data (Lineweaver-Burke, Hanes-Woolf and Eadie-Hofstee methods) or by non-linear curve fitting using GraphPad Prism (this approach is described in [71]). All curve-fitting or linearization methods had robust fit for the data points, as indicated by the R^2 values, except for Eadie-Hofstee in G3P titration (Figure 8B). Lineweaver-burke linearization was chosen for having the best fit for both NAD^+ and G3P titrations (R^2 being closest to 1).

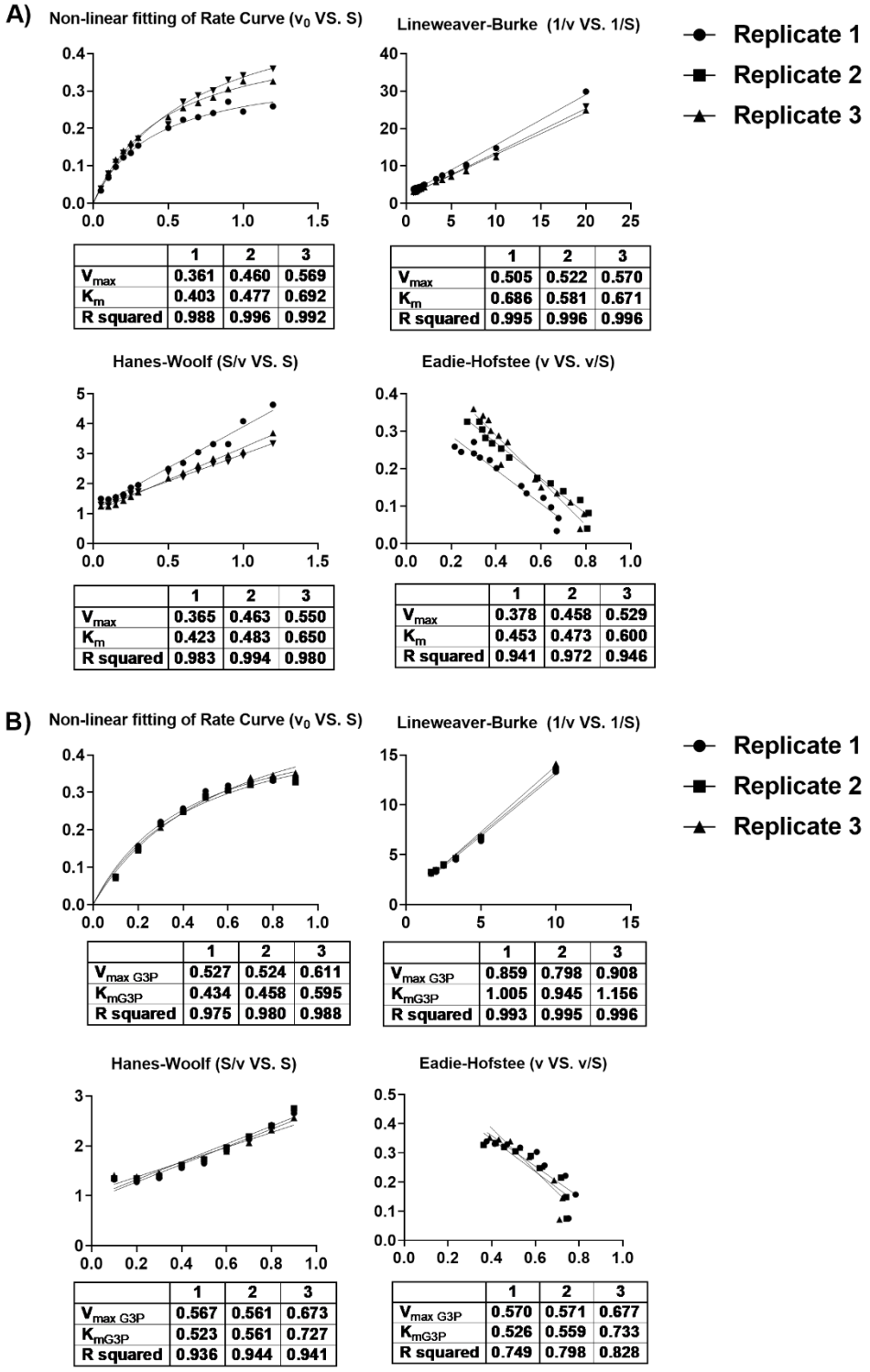

	1	2	3
V_{max}	0.361	0.460	0.569
K_m	0.403	0.477	0.692
R squared	0.988	0.996	0.992

	1	2	3
V_{max}	0.505	0.522	0.570
K_m	0.686	0.581	0.671
R squared	0.995	0.996	0.996

	1	2	3
V_{max}	0.365	0.463	0.550
K_m	0.423	0.483	0.650
R squared	0.983	0.994	0.980

	1	2	3
V_{max}	0.378	0.458	0.529
K_m	0.453	0.473	0.600
R squared	0.941	0.972	0.946

	1	2	3
$V_{max\ G3P}$	0.527	0.524	0.611
K_{mG3P}	0.434	0.458	0.595
R squared	0.975	0.980	0.988

	1	2	3
$V_{max\ G3P}$	0.859	0.798	0.908
K_{mG3P}	1.005	0.945	1.156
R squared	0.993	0.995	0.996

	1	2	3
$V_{max\ G3P}$	0.567	0.561	0.673
K_{mG3P}	0.523	0.561	0.727
R squared	0.936	0.944	0.941

	1	2	3
$V_{max\ G3P}$	0.570	0.571	0.677
K_{mG3P}	0.526	0.559	0.733
R squared	0.749	0.798	0.828

Figure 8. K_m and V_{max} calculation for substrate titrations performed with purified GAPDH in pH 7.4 native buffer. **A)** Kinetic parameter calculation of NAD^+ titration using non-linear fitting and linearization methods. **B)** Kinetic parameter calculation of G3P titration using non-linear curve fitting and linearization methods. Calculations are performed on the rate curves shown in figure 6. Three replicates were performed for each substrate titration, and each replicate was conducted in triplicates. The averaged values from the triplicates were used for calculation.

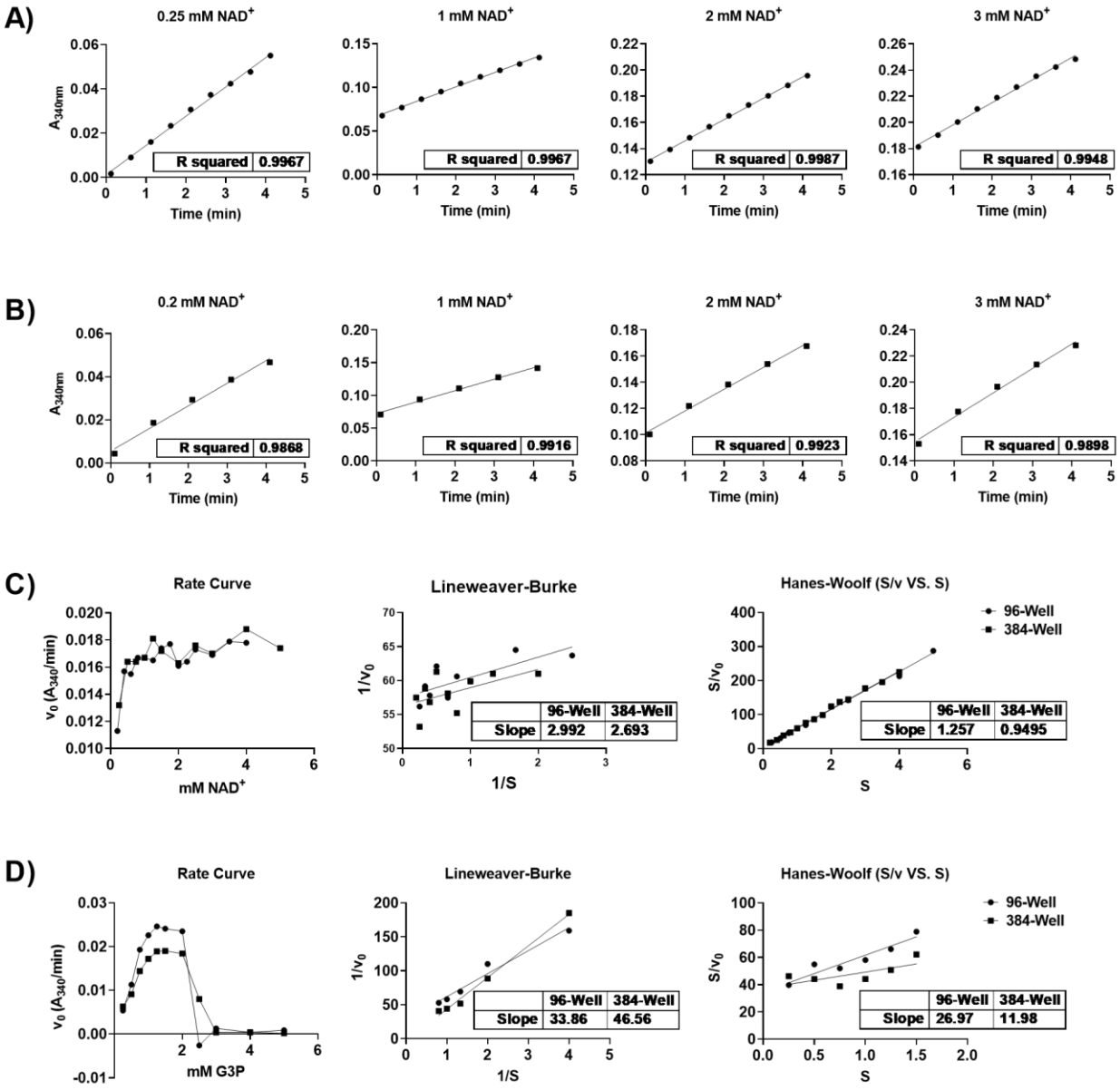

Figure 9. The 96-well and 384-well plate activity assay protocol yielded similar results for kinetic analysis of Xenopus cytoplasmic homogenate. Sample initial rates of GAPDH using the **A)** 96- and **B)** 384- well plate assay. GAPDH was assayed in pH 7.4 native buffer with one mM DTT and 5% glycerol. Michaelis-Menten rate curve and linearization for **C)** NAD^+ and **D)** G3P titration performed with rGAPDH in native buffer showed similar results for both the 96- and 384-well plate assays. The Lineweaver-Burke linearization showed less variability compared to the Hanes-Woolf method and was chosen for the future GAPDH activity analysis.

Validation of 96- and 384- well plate activity assay. Due to the turbidity of the cytoplasmic homogenate, the initial rates of cytoplasmic homogenates did not exhibit the same linearity shown by purified GAPDH. Hoping that using diluting the cytoplasmic homogenate would reduce noise in solution and better capture the initial rate, I tried to optimize the high-throughput activity assay by 1) changing the amount of sample used in existing assay protocol, and 2) modifying the final reaction volume. Based on the general GAPDH assay protocol in 384-well plates (developed by Dr. Michael Schultz and Chelsea), I refined that approach and developed and validated a similar protocol for 96-well plates. Initial rates obtained for both the 384-well plate assay and 96-well plate assay were replicable and linear (Figures 9A and 9B). The Michaelis-Menten curves obtained from the 384-well and 96-well plates appear noisier for NAD^+ titration (Figure 9C) than G3P titration (Figure 9D). Interestingly, the change in A_{340} nm between 10 to 20 minutes also formed linearity and was less noisy when plotted as the Michaelis-Menten rate curve. The Hanes-Woolf linearization yielded a better fit when compared to the Lineweaver-Burke linearization for NAD^+ titrations, while the opposite was true for G3P titrations (Figure 9C and 9D). As more assays were conducted, it became increasingly evident that the G3P rate curves were harder to linearize using the Hanes-Woolf method as the linearization often resulted in "U-shaped" curves. For easier calculation and comparison, Lineweaver-Burke linearization was chosen for future GAPDH activity analysis. Lineweaver-burke linearization is also the method of choice used in many publications [72,73,74,75]. Since no apparent differences were observed between the 96- and 384-well plate assays, the 384-well plate assay protocol was used for further experiments due to the lower sample volumes required.

3.4 Discussion

The IM with Mg^{2+} buffer had been used for biochemical studies of the oocyte nucleus and nuclear fractions. The buffer is physiological in the pH, Mg^{2+}, and Na^+ and K^+ ratio. The calcium, trace elements, and metabolites vary between cells and are not accounted for in experiments conducted for this project. The buffer pH is 7.4, corresponding to pH of cytoplasm and nucleus found in existing publications which falls withing a range of 7.2 to 7.6 [76,77,78,79]. 1 mM Mg^{2+} used in the buffer also corresponds to what has been reported for vertebrate cells [80]. The native *X. laevis* oocytes contain 144 mM potassium ions (K^+) and 19 mM sodium ions (Na^+), giving a K^+:Na^+ ratio of 7.6:1 [81]. However, the Na and K salts used for buffer preparation contain chloride (Cl^-). Recreating the native oocyte Na^+ and K^+ concentrations would result in 163 mM, which is over the total anion content of the oocyte [82,83]. 100 mM Cl^- is close to the total anion concentration in *X. laevis* oocytes, thus leading Gall *et al.* bringing down the K^+:Na^+ ratio to 5:1 (83 mM KCl, 17 mM NaCl) to a close-to-native concentration [55].

The 5:1 K^+:Na^+ ratio also approaches what has been observed in mammalian cells [84,85]. Our native buffer based on "IM with Mg^{2+}" is therefore able to create a close-to-native environment that can be used for assaying native enzyme activity in *X. laevis* homogenates.

The work described in this chapter establishes that it is possible to obtain estimates of kinetic parameters for GAPDH in homogenates of nucleus and cytoplasm in a near-native buffer. Therefore, we proceeded to obtain estimates of these parameters for the nuclear and cytoplasmic pools of GAPDH in order to test the hypothesis that the operation of GAPDH as a metabolic enzyme differs between the cytoplasm and nucleus.

Chapter 4: Kinetic differences between cytosolic and nuclear GAPDH of *X. laevis* oocytes in close-to-native conditions

4.1 Introduction

In the main introduction of this thesis (Chapter 1), we outlined that some enzymes could differ in activity between the cytoplasmic and nuclear compartment [2,3]. We pointed out that this evidence is quite limited and that the experimental approaches had some limitations. Specifically in the experiments carried out, crude estimates of initial rate without the knowledge of absolute enzyme abundance in nucleus and cytoplasm. We have also established the advantages using *X. laevis* oocyte homogenates for revisiting this question with a focus on GAPDH [20,22,21,29]. Native-western blotting of *X. laevis* homogenates revealed that cytoplasmic and nuclear GAPDH are tetrameric (Chapter 2), which has been established as the catalytically active GAPDH in literature [39]. Therefore, we know that the enzyme is potentially active in both compartments, but not whether it differs in kinetic properties between the nucleus and cytoplasm. In Chapter 3, I optimized the high-throughput activity assay protocol previously established by the Schultz lab for measuring the GAPDH activity in *X. laevis* cytoplasmic and nuclear homogenates. These robust plate assays are based on spectrophotometric measurement of the production of NAD^+, which is a classical method for kinetic analysis of GAPDH activity [40]. In this chapter we employ these says to test the central hypothesis of the thesis: The operation of GAPDH as a metabolic enzyme differs between the cytoplasm and nucleus.

4.2 Material and methods

Preparation of X. laevis homogenates and GAPDH activity assay. The preparation of cytoplasmic and nuclear homogenates and the GAPDH activity assays were performed as per section 3.2. Data obtained were analyzed using Microsoft Excel and GraphPad Prism.

4.3 Results

Chapter 3 presented validation of the assay for GAPDH in native buffer, using purified GAPDH and homogenate of oocyte cytoplasm. Here we extend that work by profiling GAPDH kinetics in nuclear and cytoplasmic homogenates. The results of the experiments shown in Figures 8 and 9 establish the kinetic behaviour of the cytoplasmic and nuclear pools of GAPDH by straightforward titration of substrates (NAD+ and G3P) into cytoplasmic and nuclear homogenates. Figure 10 is a more complex set of titrations of G3P at multiple concentrations of NAD+. The results in Figures 8-10 are for representative homogenates, not nuclear and cytoplasmic homogenates from oocytes of the same ovary isolation. The data for matched

nuclear and cytoplasmic homogenates of oocytes from four animals is shown in Figure 11. To summarize the results: the cytoplasmic and nuclear pools of GAPDH have different kinetic properties, and surprisingly, there is substantial animal-to-animal variability in how nuclear and cytoplasmic GAPDH differ in kinetic behavior.

Kinetic analysis of cytoplasmic and nuclear GAPDH using 384-well high-throughput activity assay. Using the high-throughput assay protocol established in Chapter 3, kinetic curves were obtained for nuclear and cytoplasmic GAPDH by measuring product accumulation at $A_{340\ nm}$. The concentrations of GAPDH in homogenates were calculated using mass spectrometry data and photographed volume calculations, and equal amounts of nuclear and cytoplasmic GAPDH were assayed. The kinetic curves showed that GAPDH in *Xenopus* homogenates could respond to substrate changes in the micromolar range, demonstrating high sensitivity (Figure 10).

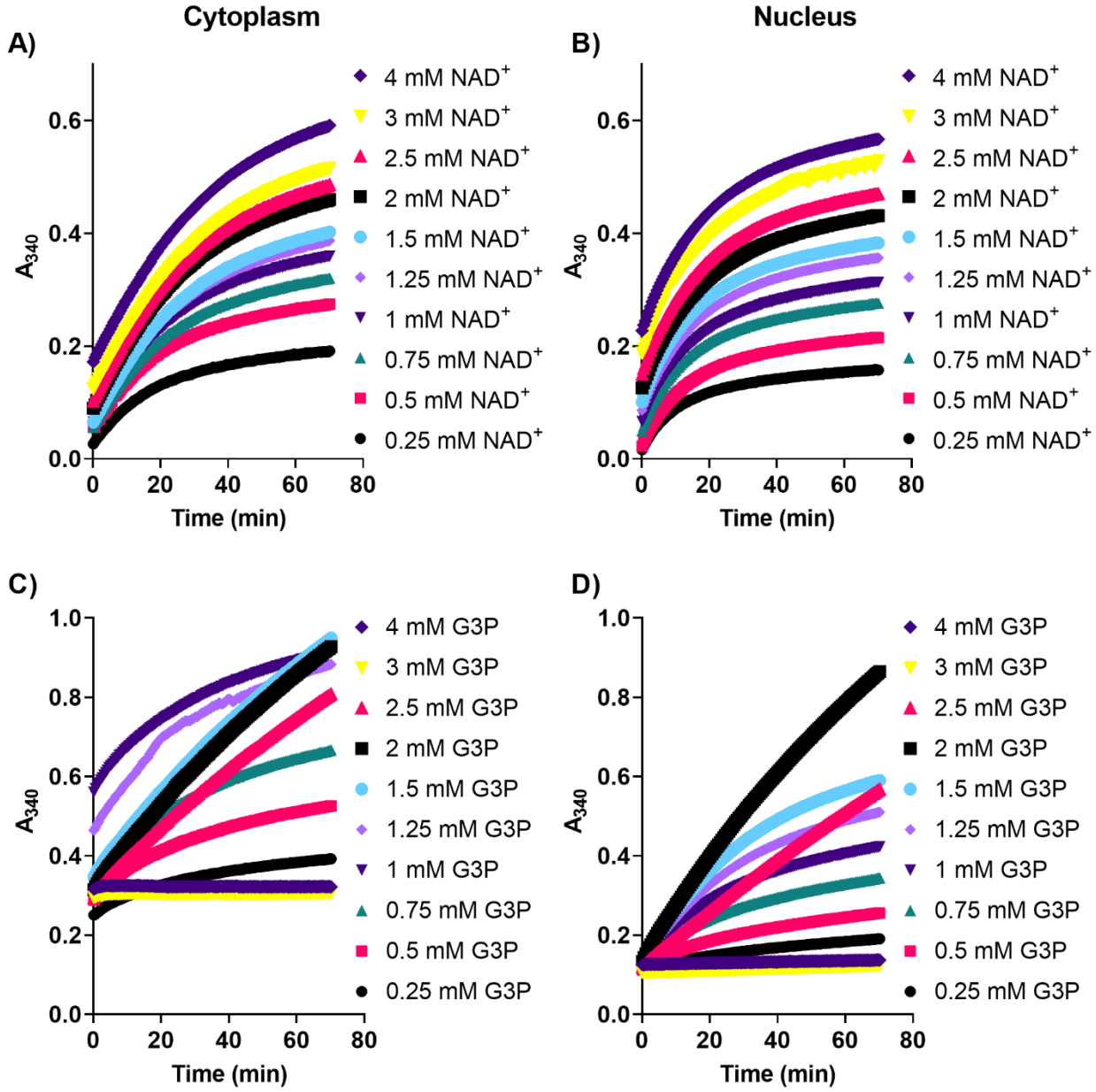

Figure 10. Sample kinetic curves obtained for X. laevis GAPDH substrate titrations in pH 7.4 native buffer. **A)** NAD^+ titration of cytoplasmic homogenates at 1 mM G3P. **B)** NAD^+ Titration of nuclear homogenates at 1 mM G3P. **C)** G3P titration of cytoplasmic homogenates at 3 mM NAD^+. **D)** G3P titration of nuclear homogenates at 3 mM NAD^+. The titrations were carried out in triplicates, and the average A_{340} between triplicates was plotted.

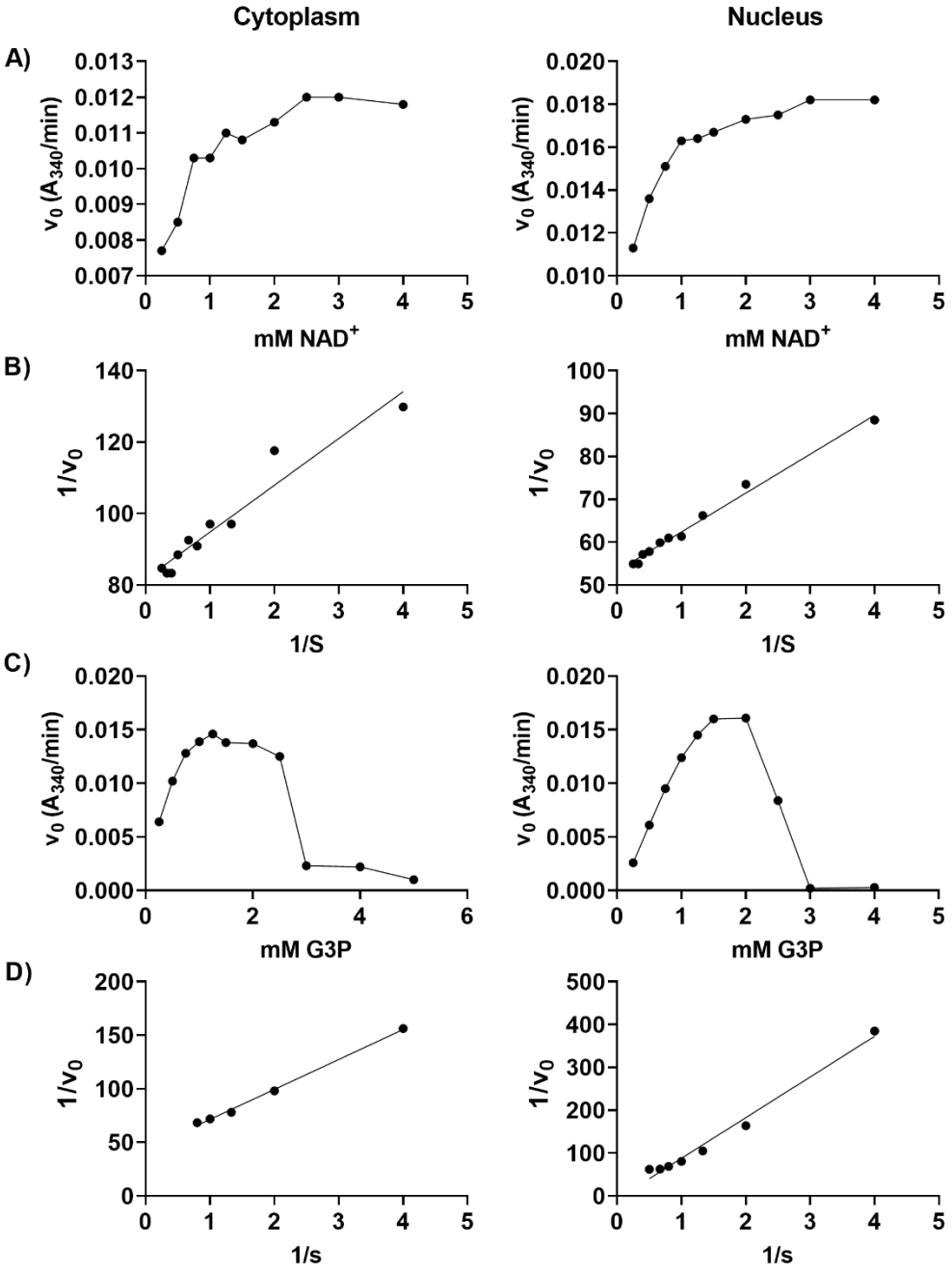

E)

	Cytoplasm		Nucleus	
	NAD^+ Titration	G3P Titration	NAD^+ Titration	G3P Titration
V_{max}	0.0124	0.0230	0.0188	-0.1426
Apparent V_{max}	0.0130	0.0145	0.0182	0.0161
K_m	0.1688	0.6425	0.1702	-13.5244

Figure 11. Sample Analysis of GAPDH K_m and V_{max} in X. laevis cytoplasmic and nuclear homogenates. The initial rates used for analysis were taken from kinetic curves shown in Figure 9. **A)** Michaelis-Menten rate curves of NAD^+ titration. **B)** Lineweaver-Burke linearization of NAD^+ titration rate curves shown in A). **C)** Michaelis-Menten rate curves of G3P titration. **D)** Lineweaver-Burke linearization of G3P titration rate curves shown in C).

As described in Chapter 3, the rate of product accumulation during the initial three minutes was linear in slope and used as the initial rate. When the initial rates were plotted, they were similar to the Michaelis-Menten rate curves of NAD^+ and G3P titrations performed with purified enzymes (Figures 11A and 11C). Despite the noise seen in the NAD^+ titrations (Figure 11A), the initial rates formed high degrees of linearity when analyzed using Lineweaver-Burke linearizations (Figure 11B). While the substrate inhibition observed on the Michaelis-Menten curves of G3P titration (Figure 11C) was similar to that of the purified enzymes, the linearization of the rate curves for calculations was much more complicated. K_m and V_{max} could be accurately calculated as high linearity using the Lineweaver-Burke method (Figure 11D). However, the calculated K_m values for G3P titration of nuclear GAPDH were occasionally negative and invalid, resulting in considerable variability between the kinetic parameters of individual experiments. This suggested that nuclear GAPDH does not fit the first-order enzyme reaction described by Lineweaver-Burke and prompted further investigation of K_m analysis. Due to the fact that in some cases K_m and V_{max} could not be calculated by linearization of the Michaelis-Menten plots, the apparent V_{max} from the rate curve was used for comparison. As shown in Figure 11, while the apparent V_{max} did not differ much between the nucleus and cytoplasm, the Lineweaver-Burke linearization suggested that the cytoplasmic GAPDH followed ideal Michaelis-Menten kinetics whereas nuclear GAPDH did not. This led us to conclude that GAPDH kinetics are different in the cytoplasmic and nuclear homogenates.

Comparing G3P titration of nuclear and cytoplasmic GAPDH at various NAD+ concentrations. While NAD^+ titration resulted in maximum *Xenopus* GAPDH activity at 3 mM NAD^+ (Figure 11A), the G3P titration performed with nuclear GAPDH often yielded negative results (Figures 11D and 11E). To follow up, we conducted the G3P titration of *Xenopus* GAPDH over a range of NAD^+ concentrations in search of better linearization results. We also experimented with analyzing rates taken from 10 to 20 minutes into the activity assay. The A_{340} collected for *X. laevis* homogenates were linear during 10 to 20 minutes after reaction initiation. Studies of enzyme kinetics also have defined initial rate as the rate taken 20 minutes after starting the reaction, "…where the changes in absorbance were in the linear range…" [86]. The shape of the Michaelis-Menten curves for remained similar for titrations conducted at all NAD^+ concentrations (Figure 12). While no significant differences were observed for nuclear GAPDH, complete substrate inhibition occurred at 3 mM G3P for titrations performed in 3- and 4- mM NAD^+ rather than 4 mM G3P (Figure 12A). This is an unexpected difference between the kinetic

behaviour of the nuclear and cytoplasmic pools of GAPDH. We have not identified the cause for this change.

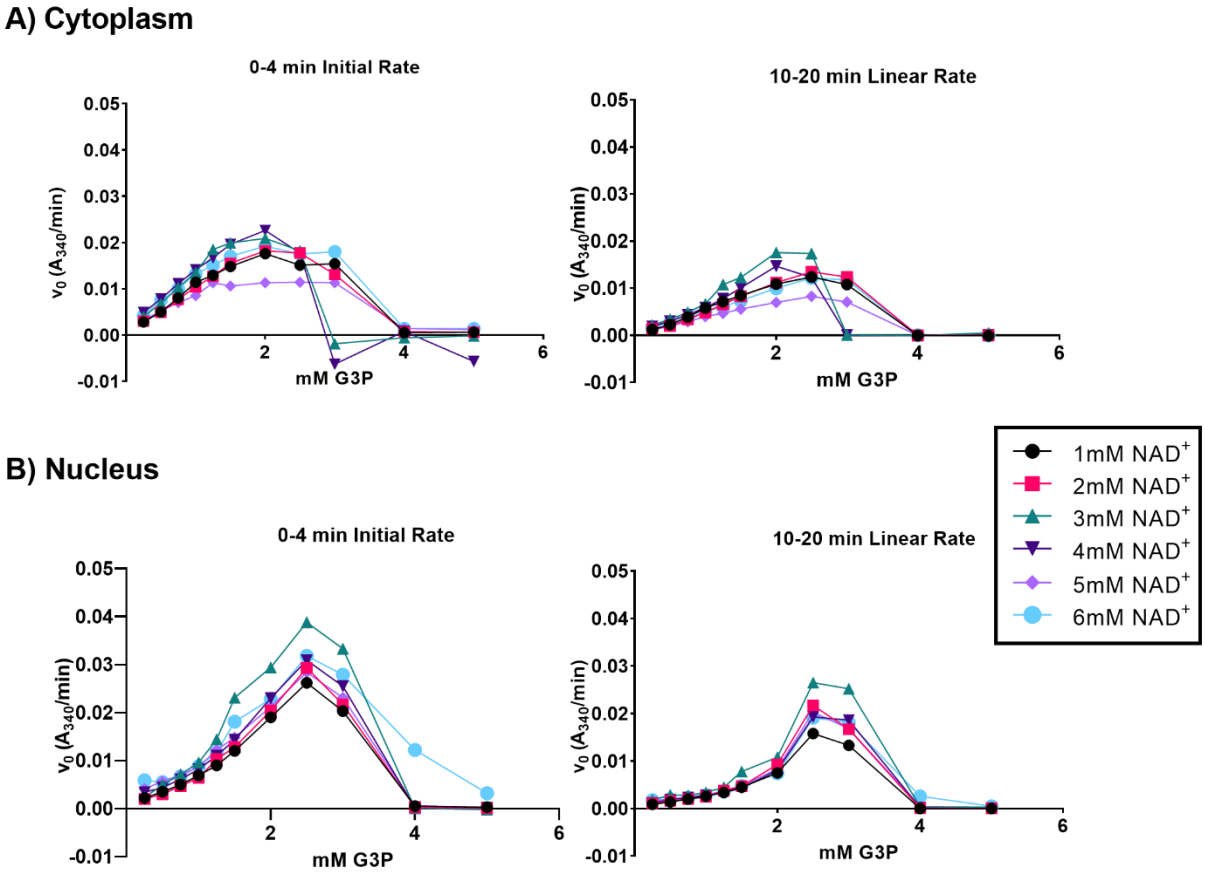

Figure 12. Comparing the nuclear and cytoplasmic GAPDH G3P titration at various NAD⁺. **A)** Michaelis-Menten rate curve of cytoplasmic GAPDH G3P titration. The overall shape of the rate curve remained similar between the experiments; in 3- and 4-mM NAD^+, complete substrate inhibition occurred at 3 mM G3P rather than 4 mM. **B)** Michaelis-Menten rate curve of nuclear GAPDH G3P titration. Overall shape of the rate curves remained similar through all concentrations of NAD^+.

There were some additional interesting points to note about the rate curves. Both cytoplasmic and nuclear GAPDH showed ideal rate curves for NAD^+ titrations. For G3P titrations, cytoplasmic GAPDH before product inhibitions exhibited a hyperbolic rate curve akin to purified enzymes (Figure 7). Nuclear GAPDH, on the other hand, displayed a more sigmoidal shape when plotted with both initial rates taken from 0 to 4 minutes and 10 to 20 minutes (Figure 12B). The sigmoidal rate curves are often observed when the target enzyme's behaviour can be influenced by the presence of effectors or regulatory compounds, where the concentration of effectors can change K_m and the apparent order of reaction [87]. The apparent

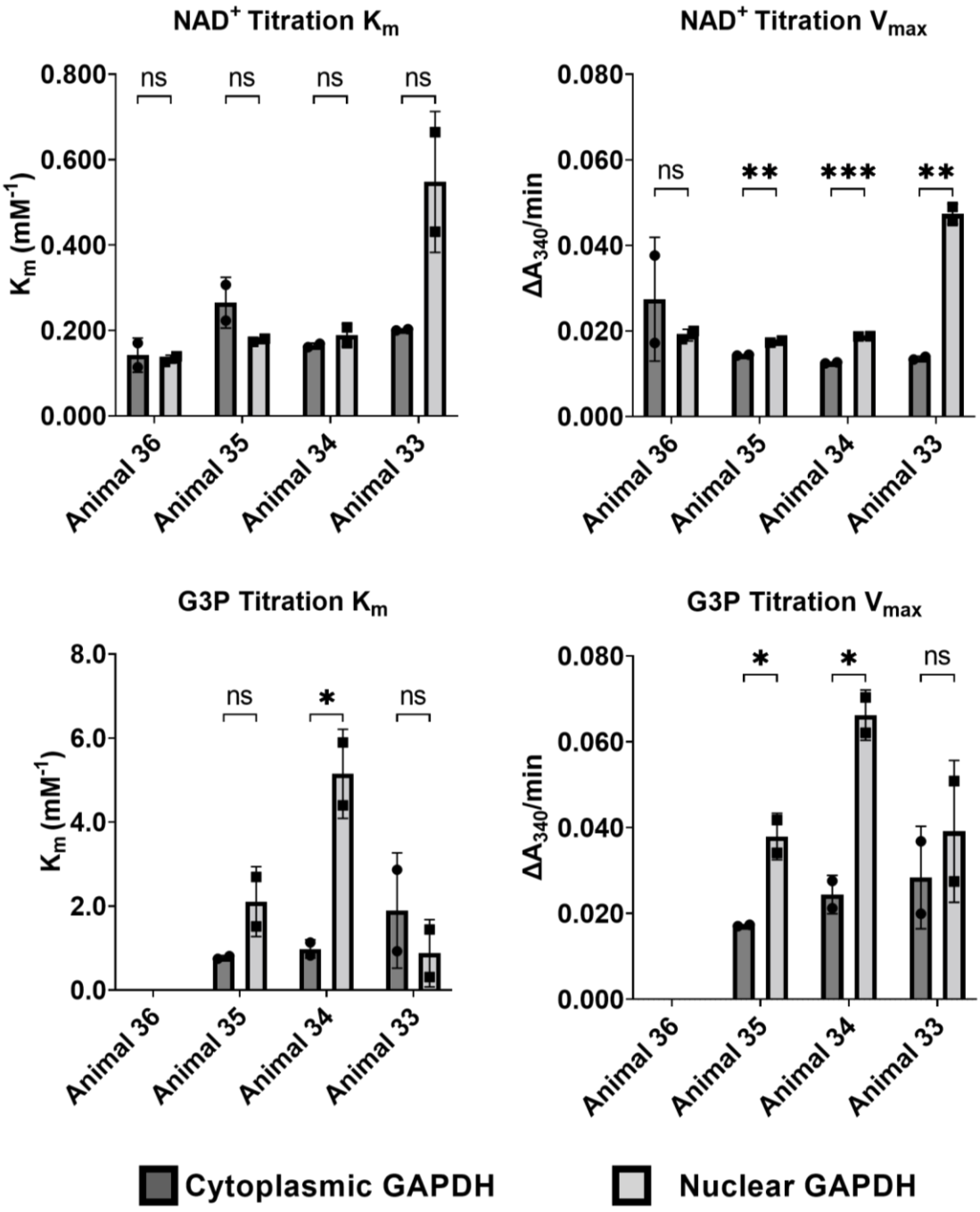

Figure 13. Separate analysis of cytoplasmic and nuclear GAPDH activity in oocytes from four different animals. Duplicate assays of GAPDH activity (with triplicate technical replicates) were performed on cytoplasmic and nuclear homogenates. All samples were prepared following the same homogenization and assay protocol. Animal 36 G3P titration kinetic parameters were not shown on the graphs due to negative values obtained using Lineweaver-Burke calculations. Independent T-tests (n_{cyto} = 2, n_{nuc} = 2) were performed on data collected for each animal. Standard deviations are shown as error bars on graphs. ns indicates no significant differences found between the values with $P > 0.05$. Asterisks mark significant differences found between values with ∗ indicating $P \leq 0.05$, ∗∗ for $P \leq 0.01$, and ∗∗∗ for $P \leq 0.001$.

V_{max} of nuclear GAPDH was higher than cytoplasmic GAPDH for G3P titrations. Despite not having specific evidence for the causation nor implication of these differences, the above observations strongly suggested that the catalytic behaviour of GAPDH differs between the cytoplasm and nucleus. In other words, the operation of GAPDH as a metabolic enzyme differs between the cytoplasm and nucleus.

A test of animal-to-animal variability of the activity signatures of nuclear and cytoplasmic GAPDH

As the assay protocol was optimized over the course of this project, the kinetic parameters obtained between animals differed. The metabolite abundance variance between oocytes [88] within an animal was addressed during our homogenate preparation, thus we wanted to determine if the differences were caused by animal-to-animal variation. Previous publications have reported phenotypical differences amongst animals with "…identical genetic background, a single source colony … as well as a single source of animal diet…" [89]. For this investigation, we performed duplicates of triplicate activity assays on cytoplasmic and nuclear homogenates harvested from four individual animals (Figure 13).

From the figure, we can see that almost all K_m and V_{max} obtained for NAD^+ titration performed with cytoplasmic and nuclear homogenates were highly reproducible within each animal. While Animal 34 to 36 had similar K_m and V_{max} values for NAD^+ titration, the GAPDH K_m and V_{max} was drastically higher in the nucleus than cytoplasm of animal 33. G3P titration was more variable due to the non-ideal Michaelis-Menten rate curves described in Figure 12. The cytoplasmic G3P titration kinetic parameters were more reproducible within each animal when compared to the nuclear kinetic parameters. While no obvious trend was observed for the K_m comparisons, the V_{max} obtained in G3P titrations was consistently higher for nuclear GAPDH than cytoplasmic GAPDH similar to what was observed when comparing the apparent V_{max} on the Michaelis-Menten rate curves (Figure 11E and 12). From this we conclude, nuclear and cytoplasmic GAPDH in *X. laevis oocytes* does differ kinetically despite the presence of animal-to-animal variability.

Chapter 5: Overall summary, implications and future directions.

5.1 Overall summary

We have established the *X. laevis* oocyte as a suitable model cell type for studying the catalytic behaviour of the pools of GAPDH in the nucleus and cytoplasm (Chapter 1).

The nuclear and cytoplasmic pools of GAPDH were shown to be in the catalytically active tetrameric form (Chapter 2). Methods for analysis of the kinetic behavior of the nuclear and cytoplasmic pools of GAPDH in a native reaction buffer were established (Chapter 3). We were able to take advantage of previous work in which nuclei and cytoplasms isolated from *X. laevis* oocytes were used to determine the absolute concentrations of all proteins in these compartments [25]. Specifically, the kinetic behavior of GAPDH could be compared by analyzing the same amounts of nuclear and cytoplasmic enzyme. This was never done in previous studies; rates were calibrated to the amount of total protein analyzed, not the actual amount of any specific enzyme [2,3].

A comprehensive series of substrate titrations revealed that the operation of GAPDH as a metabolic enzyme differs between the cytoplasm and nucleus (Chapter 4). Therefore, our work provides the first definitive evidence of catalytic regulation of a metabolic enzyme by nuclear as compared to cytoplasmic localization.

5.2 Implications

It is well established that the catalytic behaviour of GAPDH can vary between cells. Cells of different types can support different levels of flux through glycolysis and therefore different levels of GAPDH activity [90,91]. Cells of the same type can support different levels of activity depending on their physiological state. For example, treatment with reagents that induce apoptosis can cause inhibition of GAPDH activity [32,92] as well as GAPDH inhibition observed in post-ischaemic myocardium [66]. Here we show that the catalytic behaviour of GAPDH can vary within a cell depending on whether the enzyme is in the nucleus or the cytoplasm.

Our work has two main implications:

First, Compartment-specific molecular mechanisms modulate the catalytic behavior of GAPDH. As mentioned in section 4.3, the Michaelis-Menten rate curve for G3P titration of nuclear GAPDH is sigmoidal (Figure 12B). The sigmoidal curve could suggest the presence of a regulatory pathway or molecule for GAPDH that is only present in the nucleus [87]. There is a clear general precedent for this type of regulation. In hepatocytes, the glycolytic enzyme

glucokinase is catalytically inhibited in the nucleus because the nucleus is the sole location of glucokinase regulatory protein [93,94]. The latter protein is a competitive inhibitor of glucose association with glucokinase [95]. Interestingly, sigmoidal kinetics has been observed for glucokinase, though the molecular mechanism for this phenomenon is not fully understood [96].

Second, there is a biological advantage to having kinetically different pools of GAPDH in the nucleus and cytoplasm. We are not aware of studies of the kinetic behaviour of any other nucleocytosolic enzyme that might inform our thinking about what this biological advantage might be.

5.3 Future directions

The future directions to pursue relate to the two implications highlighted above:

1. Exploration of the compartment-specific molecular mechanisms that modulate the catalytic behavior of GAPDH. The activity of GAPDH is influenced by a plethora of post-translation modifications, such as phosphorylated by Ca^{2+}/calmodulin-dependent protein kinase (CaMKIIβM) [97], and binding to RNA [57,58,59,60]. A reasonable way to begin exploring compartment-specific regulation of GAPDH would be to isolate GAPDH from the nucleus and cytoplasm (pure enzyme and complexes containing GAPDH and other macromolecules). One could then systematically test any features that distinguish these enzyme pools for a role in differential enzyme regulation by subcellular location. It is also important to consider that GAPDH might be allosterically regulated by metabolites that have a different concentration in the nucleus and cytoplasm. This is an attractive possibility because evidence is mounting that some metabolites can have a local concentration that differs from the average concentration in the cell as a whole [10,98]. A specific metabolite of interest is malonyl-CoA. The activity of GAPDH is regulated by its malonylation [31]. Malonylation at lysine 213 functions as a switch that controls GAPDH binding to mRNA and availability for catalysis in the cytoplasm. A recent bioRxiv manuscript also reports binding of malonyl-CoA to GAPDH at high dilutions of the metabolite [99].
2. In the oocyte, the there are several potential biological advantages of differentially regulating GAPDH according to subcellular localization. One is to differentially control localized pools of ATP in the nucleus and cytoplasm. This hypothesis is based on a speculation of Kirli *et al.* [25] about the importance of GAPDH localization to the oocyte nucleus. The speculation is that this localization ensures ATP-generating flux through

the lower phase of glycolysis in the nucleus at the same time as there is reverse glycolytic flux in the cytosol to support glycogen synthesis. One important reason for continuous high synthesis of ATP in the oocyte relates to the turnover of acetate groups on histone molecules [100]. The maintenance of nuclear H3 and H4 in the acetylated state will require a constant supply of acetyl-CoA. Based on data collected by Kirli *et al.,* nuclear-localized enzymes in *X. laevis* oocytes that can synthesize acetyl-CoA are ACLY (59.5 nM in nucleus) and ACSS2 (ACSA; 90.0 nM in nucleus) [25]. The acetylation reaction catalyzed by both these enzymes requires ATP. Therefore, it is plausible that GAPDH activity in the nucleus supplies ATP to acetyl-CoA synthetases. In this way, GAPDH might contribute to the regulation of H3 and H4, whose modification state can profoundly influence such nuclear activities as RNA polymerase I and II transcription, DNA replication, recombination and repair.

3. An additional biological advantage of compartment-specific regulation of GAPDH could relate to the control of the epigenome, a cell function that occurs in the nucleus but not the cytoplasm. Aside from the carbon metabolites, GAPDH could participate in the maintenance of nuclear NAD^+/NADH. NAD^+ is used by many nuclear processes, including deacetylation carried out by Sirtuin proteins [101]. Theoretically, coupling the GAPDH and Sirtuin reactions allows the availability of NAD^+ for deacetylation to be controlled by the direction of the GAPDH reaction. For example, glucose starvation causes GAPDH associate with and activate Sirt1 in the nucleus, and Sirt1-mediated deacetylation can induce autophagy [102]. The sigmoidal kinetics of GAPDH in the nucleus would suggest GAPDH more sensitive to energy availability (increase in glycolytic metabolite) than in the cytoplasms. This sensitivity would increase GAPDH activity as energy sources become available again and limit the NAD^+ available for Sirt1, potentially halting or reversing autophagy initiation.

In addition, our GAPDH analysis demonstrated how *X. laevis* oocyte could be used to observe the native enzymology of the nucleus. The oocytes can serve as preliminary assessments in identifying native protein function, behaviour and association complexes. With a strong background for culturing, dissection and bioinformatics of *Xenopus oocytes* established by existing literature, the potential of research conducted with these oocytes extend to studying native pathways beyond just carbon metabolism

References

1 Busch H. Summary of Discussion on Nuclear Enzymes. Experimental Cell Research. 1963;Suppl.(9):435-438.

2 Siebert G, Humphrey GB. Enzymology of the Nucleus. In: Nord FF, editor. Advances in Enzymology and Related Areas of Molecular Biology. Vol 27. New York (NY): John Wiley & Sons, Inc.; 1965. p. 239-288.

3 Kato T, Lowry OH. Distribution of Enzymes between Nucleus and Cytoplasm of Single Nerve Cell Bodies. The Journal of Biological Chemistry. 1973;248(March 25):2044-2048.

4 Jorgens DM, Inman JL, Wojcik M, Robertson C, Palsdottir H, Tsai WT, Huang H, Bruni-Cardoso A, López CS, Bissell MJ, et al. Deep nuclear invaginations are linked to cytoskeletal filaments - integrated bioimaging of epithelial cells in 3D culture. J Cell Sci. 2017;130(1):177-189.

5 Warburg O. The Metabolism of Carcinoma Cells. The Journal of Cancer Research. 1925;9(1):148-163.

6 Liberti MV, Locasale JW. The Warburg Effect: How Does it Benefit Cancer Cells? Trends Biochem Sci. 2016;41(3):211-218.

7 Pan C, Li B, Simon MC. Moonlighting functions of metabolic enzymes and metabolites in cancer. Molecular Cell. 2021;81(18):3760-3774.

8 van der Knaap JA, Verrijzer CP. Undercover: gene control by metabolites and metabolic enzymes. Genes Dev. 2016;30(21):2345-2369.

9 Li X, Yu , Xia Y, Zheng Y, Lee JH, Li W, Lyu J, Rao G, Zhang X, Qian CN, et al. Nucleus-Translocated ACSS2 Promotes Gene Transcription for Lysosomal Biogenesis and Autophagy. Mol Cell. 2017;66(5):684-697.

10 Bulusu V, Tumanov S, Michalopoulou E, van der Broek NJ, MacKay G, Nixon C, Dhayade S, Schug ZT, Voorde JV, Blyth K, et al. Acetate Recapturing by Nuclear Acetyl-CoA Synthetase 2 Prevents Loss of Histone Acetylation during Oxygen and Serum Limitation. Cell Rep. 2017;18(3):647-658.

11 Sun RC, Dukhande VV, Zhou Z, Young LEA, Emanuelle S, Brainson CF, Gentry MS. Nuclear Glycogenolysis Modulates Histone Acetylation in Human Non-Small Cell Lung Cancers. Cell Metabolism. 2019;30(5).

12 Mowry KL. Using the Xenopus Oocyte Toolbox. Cold Spring Harb Protoc. 2020 April 1;4(2020):095844.

13 Tandon P, Conlon F, Furlow JD, Horb ME. Expanding the genetic toolkit in Xenopus: Approaches and Opportunities for Human Disease Modeling. Dev Biol. 2017;426(2):325-335.

14 Gurdon JB. The egg and the nucleus: a battle for supremacy. Development. 2013;140(12):2449-2456.

15 Hunt T. Nobel Lecture: Protein Synthesis, Proteolysis, and Cell Cycle Transitions. Biosci Rep. 2002;22:465-486.

16 Dumont JN. Oogenesis in Xenopus laevis (Daudin). I. Stages of oocyte development in laboratory maintained animals. J Morphol. 1972;136(2):153-179.

17 Liu XS, Liu X. Oocyte isolation and enucleation. Methods Mol Biol. 2006;322:31-41.

18 Wühr M, Güttler T, Peshkin L, McAlister GC, Sonnett M, Ishihara K, Groen AC, Presler M, Erickson BK, Mitchison TJ, et al. The Nuclear Proteome of a Vertebrate. Curr Biol. 2015;25(20):2663-2671.

19 Newman K, Aguero T, King ML. Isolation of Xenopus Oocytes. Cold Spring Harb Protoc. 2018;2018(2):86-91.

20 Blum M, Ott T. Xenopus: An Undervalued Model Organism to Study and Model Human Genetic Disease. Cells Tissues Organs. 2018;205(5-6):303-313.

21 Nenni MJ, Fisher ME, James-Zorn C, Pells TJ, Ponferrada VG, Chu S, Fortriede JD, Burns KA, Wang Y, Lotay V, et al. Xenbase: Facilitating the Use of Xenopus to Model Human Disease. Frontiers in Physiology. 2019;10:154.

22 Fortriede JD, Pells TJ, Chu S, Chaturvedi P, Wang D, Fisher ME, James-Zorn C, Wang Y, Nenni MJ, Burns KA, et al. Xenbase: deep integration of GEO & SRA RNA-seq and ChIP-seq data in a model organism database. Nucleic Acids Res. 2020;48(D1):D776-D782.

23 Jullien J. Analysis of Nuclear Reprogramming Following Nuclear Transfer to Xenopus Oocyte. In: Beujean N, Jammes H, Jouneau A, editors. Nuclear Reprogramming. Methods in Molecular Biology. Vol 1222. New York (NY): Humana Press; 2015. p. 71-82.

24 Paine PL, Johnson ME, Lau YT, Tluczek LJ, Miller DS. The oocyte nucleus isolated in oil retains in vivo structure and functions. Biotechniques. 1992;13(2):238-246.

25 Kirli K, Karaca S, Dehne HJ, Samwer M, Pan KT, Lenz C, Urlaub H, Görlich D. A deep proteomics perspective on CRM1-mediated nuclear export and nucleocytoplasmic partitioning. Elife. 2015;Dec 17(4):e11466.

26 Waterhouse M, Procter JB, Martin DMA, Clamp M, Barton GJ. Jalview Version 2—a multiple sequence alignment editor and analysis workbench. Bioinformatics. 2009;25(9):1189-1191.

27 Jumper J, Evans R, Pritzel A, Green T, Figurnov M, Ronneberger O, Tunyasuvunakool K, Bates R, Žídek A, Potapenko A, et al. Highly accurate protein structure prediction with AlphaFold. Nature. 2021;596:583-589.

28 Pettersen EF, Goddard TD, Huang CC, Meng EC, Couch GS, Croll TI, Morris JH, Ferrin TE. UCSF ChimeraX: Structure visualization for researchers, educators, and developers. Protein Sci. 2021;30(1):70-82.

29 White MR, Garcin ED. D-Glyceraldehyde-3-Phosphate Dehydrogenase Structure and Function. In: Macromolecular Protein Complexes. Vol 83. Springer, Cham; 2017. p. 413-453.

30 Sirover MA. Pleiotropic effects of moonlighting glyceraldehyde-3-phosphate dehydrogenase (GAPDH) in cancer progression, invasiveness, and metastases. Cancer and Metastasis Reviews. 2018;37:665-676.

31 Galván-Peña S, Carroll G, Newman C, Hinchy C, Palsson-McDermott E, Robinson EK, Covarrubias S, Nadin A, James AM, Haneklaus M, et al. Malonylation of GAPDH is an inflammatory signal in macrophages. Nat Commun. 2019;10(1):338.

32 Jarosz AP, Wei W, Gauld JW, Auld J, Özcan F, Aslan M, Mutus B. Glyceraldehyde 3-phosphate dehydrogenase (GAPDH) is inactivated by S-sulfuration in vitro. Free Radic Biol Med. 2015;89(December):512-521.

33 Colell A, Green DR, Ricci JE. Novel roles for GAPDH in cell death and carcinogenesis. Cell Death Differ. 2009;16:1573-1581.

34 Hara MR, Agrawal N, Kim SF, Cascio MB, Fujimuro M, Ozeki Y, Takahashi M, Cheah JH, Tankou SK, Hester LD, et al. S-nitrosylated GAPDH initiates apoptotic cell death by nuclear translocation following Siah1 binding. Nat Cell Biol. 2005;7:665-674.

35 Nott A, Watson PM, Robinson JD, Crepaldi L, Riccio A. S-Nitrosylation of histone deacetylase 2 induces chromatin remodelling in neurons. Nature. 2008;455(7211):411-415.

36 Sen N, Synder SH. Neurotrophin-mediated degradation of histone methyltransferase by S-nitrosylation cascade regulates neuronal differentiation. Proc Natl Acad Sci USA. 2011;108(50):20178-20183.

37 Kanai H, Sawa A, Chen RW, Leeds P, Chuang DM. Valproic acid inhibits histone deacetylase activity and suppresses excitotoxicity-induced GAPDH nuclear accumulation and apoptotic death in neurons. Pharmacogenomics J. 2004;4(5):336-344.

38 Kunjithapatham R, Geschwind JF, Devine L, O'Meally RN, Cole NR, Torbenson MS, Boronina TN. Occurrence of a Multimeric High-Molecular-Weight Glyceraldehyde-3-phosphate Dehydrogenase in Human Serum. J. of Proteome Res. 2015;14:1645-1656.

39 Constantinides SM, Deal Jr. WC. Reversible Dissociation of Tetrameric Rabbit Muscle Glyceraldehyde 3-Phosphate Dehydrogenase into Dimers or Monomers by Adenosine Triphosphate. The Journal of Biological Chemistry. 1969;244(20):5695-5702.

40 Furfine CS, Velick SF. The Acyl-enzyme Intermediate and the Kinetic Mechanism of the Glyceraldehyde 3-Phosphate Dehydrogenase Reaction. J Biol Chem. 1965;271(8):844-855.

41 Betz A, Chance B. Phase Relationship of Glycolytic Intermediates in Yeast Cells with Oscillatory Metabolic Control. Arch of Biochem Biophys. 1965;109(3):585-594.

42 Révillion F, Pawlowski V, Hornez L, Peyrat JP. Glyceraldehyde-3-phosphate dehydrogenase gene expression in human breast cancer. Eur J Cancer. 2000;36(8):1038-1042.

43 Kornberg MD, Bhargava P, Kim PM, Pulturi V, Snowman AM, Putluri N, Calabresi PA, Snyder SH. Dimethyl fumarate targets GAPDH and aerobic glycolysis to modulate immunity. Science. 2018;360(6387):449-453.

44 Hoagland Jr. VD, Teller DC. Influence of Substrates on the Dissociation of Rabbit Muscle D-Glyceraldehyde 3-Phosphate. Biochemistry. 1969;8(2):594-620.

45 Traut TW. Dissociation of Enzyme Oligomers: A Mechanism for Allosteric Regulation. Critical Reviews in Biochemistry and Molecular Biology. 1994;29(2):125-163.

46 Nakajima H, Itakura M, Kubo T, Kaneshige A, Harada N, Izawa T, Azuma YT, Kuwamura M, Yamaji R, Takeuchi T. Glyceraldehyde-3-phosphate Dehydrogenase (GAPDH) Aggregation Causes Mitochondrial Dysfunction during Oxidative Stress-induced Cell Death. J Biol Chem. 2017;292(11):4727-4742.

47 Colell A, Green DR, Ricci JE. Novel roles for GAPDH in cell death and carcinogenesis. Cell Death Differ. 2009;16(12):1573-1581.

48 Crane RF, Ruderman JV. Using Xenopus oocyte extracts to study signal transduction. In: Liu XJ. Xenopus Protocols. Vol 322. Totowa (NJ): Humana Press Inc.; 2006. p. 435-443.

49 Eppig J, Steckman ML. Comparison of exogenous energy sources for in vitro maintenance of follicle cell-free Xenopus laevis oocytes. In Vitro. 1976;12(3):173-179.

50 Dworkin MB, Segil N, Dworkin-Rastl E. Pyruvate kinase isozymes in oocytes and embryos from the frog Xenopus laevis. Comp Biochem Physiol B. 1987;88(3):743-749.

51 Dworkin MB, Dworkin-Rastl E. Metabolic regulation during early frog development: glycogenic flux in Xenopus oocytes, eggs, and embryos. Dev Biol. 1989;132(2):512-523.

52 Halley-Stott RP, Pasque V, Astand C, Miyamoto K, Simeoni I, Jullien J, Gurdon JB. Mammalian nuclear transplantation to Germinal Vesicle stage Xenopus oocytes - a method for quantitative transcriptional reprogramming. Methods. 2021;51(1):56-65.

53 Sive HL, Grainger RM, Harland M. Defolliculation of Xenopus oocytes. Cold Spring Harb Protoc. 2010;2010(12):pdb.prot5535.

54 Mir A, Heasman J. How the mother can help: studying maternal Wnt signaling by anti-sense-mediated depletion of maternal mRNAs and the host transfer technique. Methods Mol Biol. 2008;469:417-429.

55 Gall JG, Murphy C, Callan HG, Wu ZA. Lampbrush chromosomes. Methods Cell Biol. 1991;36:149-166.

56 Karpel RL, Burchard AC. A basic isozyme of yeast glyceraldehyde-3-phosphate dehydrogenase with nucleic acid helix-destabilizing activity. Biochim Biophys Acta. 1981;654(2):256-267.

57 Ryazanov AG. Glyceraldehyde-3-phosphate dehydrogenase is one of the three major RNA-binding proteins of rabbit reticulocytes. FEBS Lett. 1985;192(1):131-134.

58 Parker R, Song H. The enzymes and control of eukaryotic mRNA turnover. Nat Struct Mol Biol. 2004;11(2):121-127.

59 White MR, Garcin ED. The sweet side of RNA regulation: glyceraldehyde-3-phosphate dehydrogenase as a noncanonical RNA-binding protein. Wiley Interdiscip Rev RNA. 2016;7(1):53-70.

60 Nagy E, Rigby WF. Glyceraldehyde-3-phosphate Dehydrogenase Selectively Binds AU-rich RNA in the NAD+-binding Region (Rossmann Fold). J Biol Chem. 1995;270(6):2755-2763.

61 Carmona P, Rodriguez-Casado A, Molina M. Conformational structure and binding mode of glyceraldehyde-3-phosphate dehydrogenase to tRNA studied by Raman and CD spectroscopy. Biochim Biophys Acta. 1999;1432(2):222-233.

62 Demarse NA, Ponnusamy S, Spicer EK, Apohan E, Baatz E, Ogretmen B, Davies C. Direct binding of glyceraldehyde 3-phosphate dehydrogenase to telomeric DNA protects telomeres against chemotherapy-induced rapid degradation. J Mol Biol. 2009;394(4):789-803.

63 Yang W, Xia Y, Ji H, Zheng Y, Liang J, Huang W, Gao X, Aldape K, Lu Z. Nuclear PKM2 regulates β-catenin transactivation upon EGFR activation. Nature. 2011;408(7375):118-122.

64 Yang W, Zheng Y, Xia Y, Ji H, Chen X, Guo F, Lyssiotis CA, Aldape K, Cantley LC, Lu Z. ERK1/2-dependent phosphorylation and nuclear translocation of PKM2 promotes the Warburg effect. Nat Cell Biol. 2012;14(12):1295-1305.

65 Gao X, Wang H, Jenny JY, Liu X, Liu ZR. Pyruvate Kinase M2 Regulates Gene Transcription by Acting as A Protein Kinase. Mol Cell. 2012;45(5):598-609.

66 Knight RJ, Kofoed KF, Schelbert HR, Buxton DB. Inhibition of glyceraldehyde-3-phosphate dehydrogenase in post-ischemic myocardium. Cardiovascular Research. 1996;32(6):1016-1023.

67 Gall JG, Wu Z. Examining the Contents of Isolated Xenopus Germinal Vesicles. Methods. 2010;51(1):45-51.

68 Maurer JB, Bovo F, Gomes EM, Loureiro HM, Stevan FR, Zawadzki-Baggio SF, Nakano M. Kinetic Data of D-Glyceraldehyde-3-phosphate Dehydrogenase from HeLa Cells. Current Enzyme Inhibition. 2015;11(2):124-131.

69 Shinyashiki M, Rodriguez CE, Di Stefano EW, Sioutas C, Delfino RJ, Kumagai Y, Froines JR, Cho AK. On the interaction between glyceraldehyde-3-phosphate dehydrogenase and airborne particles: Evidence for electrophilic species. Atmospheric Environment. 2008;42(3):517-529.

70 Tummler K, Lubitz T, Schelker M, Klipp E. New types of experimental data shape the use of enzyme kinetics for dynamics network modeling. FEBS Journal. 2014;281(2):549-571.

71 Kemmer G, Keller S. Nonlinear least-squares data fitting in Excel spreadsheets. Nature Protocols. 2010;5:267-281.

72 Errafiy N, Soukri A. Purification and partial characterization of glyceraldehyde-3-phosphate dehydrogenase from the ciliate Tetrahymena thermophila. Acta Biochim Biophys Sin (Shanghai). 2012;44(6):527-534.

73 Zhu W, Zhang Q, Li J, Wei Y, Cai C, Liu L, Xu Z, Jin M. Glyceraldehyde-3-phosphate dehydrogenase acts as an adhesin in Erysipelothrix rhusiopathiae adhesion to porcine endothelial cells and as a receptor in recruitment of host fibronectin and plasminogen. Vet Res. 2017;48(1):16.

74 Puder M, Soberman RJ. Glutathione Conjugates Recognize the Rossmann Fold of Glyceraldehyde-3-phosphate Dehydrogenase. J Biol Chem. 1997;272(16):10936-10940.

75 Madureira P, Baptista M, Vieria M, Magalhães V, Camelo A, Oliveira L, Ribeiro A, Tavares D, Trieu-Cuot P, Vilanova M, et al. Streptococcus agalactiae GAPDH is a virulence-associated immunomodulatory protein. J Immunol. 2007;178(3):1379-1387.

76 Casey J, Grinstein S, Orlowski J. Sensors and regulators of intracellular pH. Nat Rev Mol Cell Biol. 2010;11:50-61.

77 Milo R, Jorgensen PC, Moran U, Weber GM, Springer M. BioNumbers—The database of key numbers in molecular and cell biology. Nucleic Acids Research. 2010;38(suppl 1):D750-D753.

78 Masuda A, Oyamada M, Nagaoka T, Tateishi N, Takamatsu T. Regulation of cytosol-nucleus pH gradients by K+/H+ exchange mechanism in the nuclear envelope of neonatal rat astrocytes. Brain Res. 1998;807(1-2):70-77.

79 Tantama M, Hung YP, Yellen G. Imaging intracellular pH in live cells with a genetically encoded red fluorescent protein sensor. J Am Chem Soc. 2011;133(26):10034-10037.

80 Romani A, Scarpa A. Regulation of cell magnesium. Arch Biochem Biophys. 1992;298(1):1-12.

81 Horowitz SB, Miller DS. Solvent properties of ground substance studied by cryomicrodissection and intracellular reference-phase techniques. J Cell Biol. 1984;99(1 Pt 2):172s-179s.

82 Kusano K, Miledi R, Stinnakre J. Cholinergic and catecholaminergic receptors in the Xenopus oocyte membrane. J Physiol. 1982;328:143-170.

83 O'Connor CM. Analysis of aspartic acid and asparagine metabolism in Xenopus laevis oocytes using a simple and sensitive HPLC method. Mol Reprod Dev. 1994;39(4):392-396.

84 Brant L, Georgomanolis T, Nikolic M, Brackley CA, Kolovos P, van Ijcken W, Grosveld FG, Marenduzzo D, Papantonis A. Exploiting native forces to capture chromosome conformation in mammalian cell nuclei. Mol Syst Biol. 2016;12(12):891.

85 Kimura H, Tao Y, Roeder RG, Cook PR. Quantitation of RNA polymerase II and its transcription factors in an HeLa cell: little soluble holoenzyme but significant amounts of polymerases attached to the nuclear substructure. Mol Cell biol. 1999;19(8):5383-5392.

86 Kerr GA, Wang Z, Wang N, Kwok KHM, Jalkanen J, Ludzki A, Lecoutre S, Langin D, Bergo MO, Dahlman I, et al. The long noncoding RNA ADIPINT regulates human adipocyte metabolism via pyruvate carboxylase. Nat Commun. 2022;13(1):2958.

87 Atkinson DE, Walton GM. KINETICS OF REGULATORY ENZYMES. ESCHERICHIA COLI PHOSPHOFRUCTOKINASE. J Biol Chem. 1965;240:757-763.

88 Vastag L, Jorgensen P, Peshkin L, Wei R, Rabinowitz JD, Kirschner MW. Remodeling of the metabolome during early frog development. PLoS One. 2011;6(2):e16881.

89 Corrigan JK, Ramachandran D, He Y, Palmer CJ, Jurczak MJ, Chen R, Li B, Friedline RH, Kim JK, Ramsey JJ, et al. A big-data approach to understanding metabolic rate and response to obesity in laboratory mice. Elife. 2020;9:e53560.

90 Shestov AA, Liu X, Ser Z, Cluntun AA, Hung YP, Huang L, Kim D, Le A, Yellen G, Albeck JG, et al. Quantitative determinants of aerobic glycolysis identify flux through the enzyme GAPDH as a limiting step. eLife. 2014;3:e03342.

91 Pike Winer LS, Wu M. Rapid analysis of glycolytic and oxidative substrate flux of cancer cells in a microplate. PLoS One. 2014;9(10):e109916.

92 Shenton D, Grant CM. Protein S-thiolation targets glycolysis and protein synthesis in response to oxidative stress in the yeast Saccharomyces cerevisiae. Biochem J. 2003;374(Pt 2):513-519.

93 Shiota C, Coffey J, Grimsby J, Grippo JF, Magnuson MA. Nuclear Import of Hepatic Glucokinase Depends upon Glucokinase Regulatory Protein, whereas Export Is Due to a Nuclear Export Signal Sequence in Glucokinase. J Biol Chem. 1999;274(52):37125-37130.

94 Iynedjian PB. Molecular Physiology of Mammalian Glucokinase. Cell Mol Life Sci. 2009;66(1):27-42.

95 Sternisha SM, Miller BG. Molecular and cellular regulation of human glucokinase. Arch Biochem Biophys. 2020;663:199-213.

96 Kamata K, Mitsuya M, Nishimura T, Eiki Ji, Nagata Y. Structural Basis for Allosteric Regulation of the Monomeric Allosteric Enzyme Human Glucokinase. Structure. 2004;12(3):429-438.

97 Singh P, Salih M, Leddy JJ, Tuana BS. The Muscle-specific Calmodulin-dependent Protein Kinase Assembles with the Glycolytic Enzyme Complex at Sarcoplasmic Reticulum and Modulates the Activity of Glyceraldehyde-3-phosphate Dehydrogenase in a Ca2+/Calmodulin-dependent Manner. J Biol Chem. 2004;279(34):35176-35182.

98 Sutendra G, Kinnaird A, Dromparis P, Paulin R, Stenson H, Harmony A, Hashimoto K, Zhang N, Flaim E, Michelakis ED. A nuclear pyrucate dehydrogenase complex is important for generation of acetyl-CoA and histone acetylation. Cell. 2014;158(1):84-97.

99 Hicks KG, Cluntun AA, Schubert HL, Hackeet SR, Berg JA, Leonard PG, Ajalla Aleixo MA, Belvins A, Barta P, Tilley S, et al. Protein-Metabolite Interactomics Reveals Novel Regulation of Carbohydrate Metabolism. BioRxiv. 2021.

100 Woodland HR. The modification of stored histones H3 and H4 during the oogenesis and early development of Xenopus laevis. Developmental Biology. 1979;68(2):360-370.

101 Carafa V, Rotili D, Forgione M, Cuomo F, Serretiello E, Hailu GS, Jarho E, Lahtela-Kakkonen M, Mai A, Altucci L. Sirtuin functions and modulation: from chemistry to the clinic. Clin Epigenet. 2016;8(61):eCollection.

102 Chang C, Su H, Zhang D, Wang Y, Shen Q, Liu B, Huang R, Zhou T, Peng C, Wong CCL, et al. AMPK-Dependent Phosphorylation of GAPDH Triggers Sirt1 Activation and Is Necessary for Autophagy upon Glucose Starvation. Mol Cell. 2015;60(6):930-940.

103 Gurdon JB, Wickens MP. The use of Xenopus oocytes for the expression of cloned genes. Methods Enzymol. 1983;101:370-386.

104 Elias H, Hyde DM. A Guide to Practical Stereology. Basel ; New York: Karger; 1983.

Supplemental Material

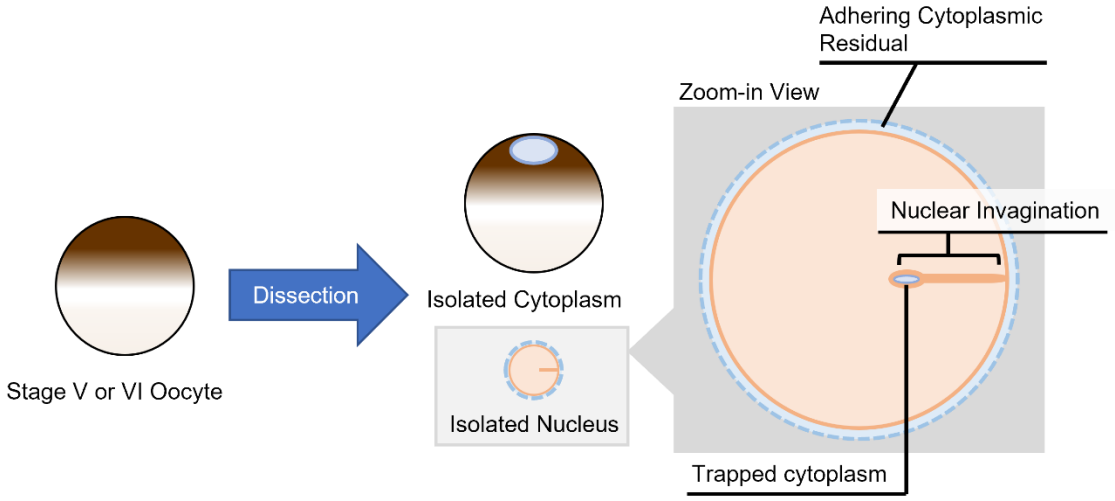

Figure S1 Association of cytoplasmic material with nuclei dissected from of X. laevis oocytes. *X. laevis* oocytes were dissected while immersed in mineral oil at room temperature (25℃). Nuclear isolation using these oocytes does not eliminate the cytoplasmic material trapped within deep nuclear invaginations. From images of the *X. laevis* oocytes in existing literature *[24,103]*, the residual cytoplasm isolated with the nucleus is estimated by the "point-hit" method *[104]* to be 4% of the nuclear volume. Using the Kirli *et al.* protein concentrations *[25],* approximately only 0.01% of GAPDH in the isolated nucleus originates from associated cytoplasmic material.